Title

THE EFFECT OF IMPROVING ENERGY RESOLUTION ON GAMMA CAMERA PERFORMANCE: A QUANTITATIVE ANALYSIS

Authors

Llacer, Jorge
Graham, L. Stephen.

Publication Date

1974-12-01

Presented at the Nuclear Science Symposium, Washington, D.C., December 11-13, 1974.

LBL-3631

THE EFFECT OF IMPROVING ENERGY RESOLUTION ON GAMMA CAMERA PERFORMANCE: A QUANTITATIVE ANALYSIS

Jorge Llacer and L. Stephen Graham

December 1974

Prepared for the U. S. Atomic Energy Commission under Contract W-7405-ENG-48

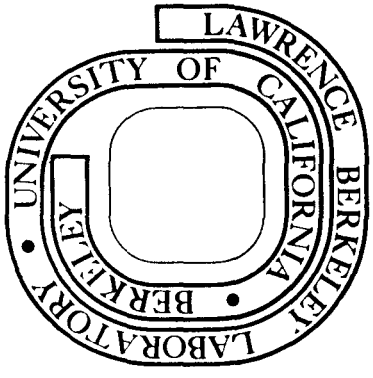

DISCLAIMER

THE EFFECT OF IMPROVING ENERGY RESOLUTION ON GAMMA CAMERA PERFORMANCE: A QUANTITATIVE ANALYSIS*

Jorge Llacer

Lawrence Berkeley Laboratory
University of California
Berkeley, California 94720

and

L. Stephen Graham

Department of Radiological Sciences
Nuclear Medicine Division
University of California, Los Angeles

ABSTRACT

The Modulation Transfer Functions (MTF) of two commercial cameras and of a single element germanium camera fitted with different collimator configurations have been studied theoretically and experimentally in order to separate the different elements which contribute to the imaging capabilities of a gamma camera. Effects due to size and shape of collimator holes, and to positron range at 511 keV have been treated as filtering functions, predicting the behavior of a camera quite accurately. The effect of energy resolution has then been studied by noting the changes in MTF and the corresponding changes in the computer generated image of a low contrast circularly symmetric phantom as a function of energy resolution. The possibility of excellent imaging under low contrast situations with high-energy resolution detectors is demonstrated, and the required penalty in camera speed is documented.

INTRODUCTION

It has commonly been understood that the elimination of scattered radiation in radioisotope imaging results in a desirable improvement in image contrast. Beck, et al[1] first presented an analysis of the tradeoff between efficiency and contrast by energy discrimination in conventional scanners. That work led one of the authors (Llacer)[2] to undertake a detailed quantitative analysis of the effects of energy resolution on the imaging capabilities of rectilinear scanners. It was found that the good energy resolution of germanium detectors makes it possible to construct scanners with spatial resolution in the millimeter range with good contrast. The main penalty for such high resolution would be a loss of scanning speed, to the point that such scanners would become more useful as specialized tools for detailed scanning of small regions in humans or animals rather than instruments for routine diagnosis. The concept of a germanium camera with a multi-hole, parallel-wall collimator was first proposed by Parker, et al[3] and has been extended by other workers[4-7] using different configurations. In all cases, results have been encouraging in the sense that imaging is possible with good spatial resolution, although the cameras have small fields of view.

The increased activity in this field must be based on the premise that specific advantages are to be gained in a gamma camera by the use of high resolution detectors, apart from the obvious ability to image several isotopes, or isotopes with several photopeaks, simultaneously. For a rectilinear scanner, in which the field of view of a focusing collimator may include a large conical region of tissue from which radiation can be scattered into the detector, energy resolution has been found to be of substantial importance.[1] A single hole of a multi-hole, parallel-wall collimator, however, often views a much smaller region from which radiation can be scattered; it would seem, therefore, that scattering is then a less important factor in determining camera performance than in the case of a scanner.

The object of this paper to separate the different elements which determine camera performance in static imaging and to isolate specifically the effects of energy resolution. A theoretical study in terms of the modulation transfer function (MTF) of a camera is done first, and measurements with a single-element germanium camera are used to complete the analytical part of the study. The performances of two commercial camera systems are then presented in light of that analysis and computer generated images are shown relating the measured MTFs of the commercial cameras and of the one-element germanium camera to photographic images. The paper concludes with a discussion of the specific advantages and disadvantages of high resolution cameras and of optimum design considerations.

THEORETICAL ANALYSIS OF THE ELEMENTS CONSTITUTING THE MODULATION TRANSFER FUNCTION

A gamma camera with a multi-hole, parallel-wall collimator, whether it has a detector consisting of multiple crystals or a single, large diameter, flat crystal, can be described as a "sampling" system. In

* This work was supported, in part, by the U.S. Atomic Energy Commission under Contract AT(04-1)GEN-12

The experimental work described here was carried out at the Laboratory of Nuclear Medicine and Radiation Biology at UCLA.

fact, the collimator will sample the source radiation distribution at points separated by a sampling distance d_s. For such systems the Sampling Theorem of linear systems provides a very convenient framework for studying imaging properties. For intensity variations in one direction only, the Sampling Theorem can be stated as follows:

"Consider a source distribution s(x) with a spectrum of frequencies $S(\nu_x)$ which becomes zero above a cut-off frequency ν_c. Then, the source s(x) can be reconstructed identically by sampling the distribution at points separated by a sampling distance $d_s = 1/2\ \nu_c$ in the x-direction and computing s(x) from

$$s(x) = \sum_n s\left(\frac{n}{2\nu_c}\right) \cdot \text{sinc}\ 2\nu_c\left(x - \frac{n}{2\nu_c}\right) \qquad (1)$$

where $-\infty < n < \infty$, the function sinc $(\beta) = (\sin \pi\beta)/\pi\beta$, and $s(n/2\nu_c)$ is the value of the function at points separated by the sampling distance."

The implication of Eq. (1) is that it is not necessary to know the activity at all points of a band limited distribution, but only at discrete values of x. Carrying out the sampling at points separated by a distance larger than $1/2\ \nu_c$ results in a loss of information. On the other hand, sampling distances smaller than the critical value produce redundant information, but give improved counting rates and therefore improved statistics.

In gamma-ray scintigraphy we have to look at the sampling theorem from a different perspective. The information contained in the source s(x) is not band limited, in general, but we observe it with a collimator which samples at a distance interval d_s. We can conclude from Eq. (1) that information contained in source frequencies below $\nu_c = 1/2\ d_s$ can be reproduced exactly by such a collimator system. Information contained at $\nu \geq \nu_c$ will produce a system response which may be totally meaningless. For example, a sine wave with $\nu = \nu_c$ exactly cannot be distinguished from zero by sampling at the zero crossing points, and sine waves with $\nu > \nu_c$ are reproduced as sine waves of $\nu < \nu_c$ with phases depending on ν and ν_c. A basic property of a collimator design therefore emerges: if the distance between collimator holes in a given direction is d_s, the largest frequency that can be observed meaningfully in that direction is $\nu_c < 1/2\ d_s$. The sinc function of Eq. (1) is not used to generate images in camera systems. Rather, square waves or dot patterns are generated. The basic capability defined by Eq. (1) stands as an upper limit, neverthless; it can be proven that no sampling waveform can reproduce a source s(x) more accurately than the sinc function, or reproduce information correctly above a frequency $\nu_c = 1/2\ d_s$.

For efficient detection, the sampling points seen by the collimator are not infinitesimally small, as the sampling theorem of Eq. (1) implies. Finite hole sizes and collimator thicknesses are used, so that the sampling is done over a field of view. If we assume that for a given collimator and source-to-collimator distance the field of view sampled by one hole in one direction has a particular length 2L, and letting $h_w(x)$ define the weight given by the system geometry to the activity existing in the field of view of the hole, we find that instead of $s(n/2\nu_c)$ of Eq. (1), the intensity measured at a particular point n is

$$I\left(\frac{n}{2\nu_c}\right) = \int_{\frac{n}{2\nu_c} - L}^{\frac{n}{2\nu_c} + L} h_w\left(x - \frac{n}{2\nu_c}\right) s(x)\ dx \qquad (2)$$

Since $h_w(x) = 0$ outside of $x = \pm L$, the limits of integration can be extended to $\pm \infty$ and Eq. (2) becomes a convolution of s(x) with the weighting function $h_w(x)$. The effect of finite hole size can, therefore, be described as a pre-filtering of the source by $h_w(x)$ followed by perfect sampling. Figure 1 shows schematically the upper frequency limit ν_c of a camera with sampling points separated by d_s = 0.277 cm (Baird-Atomic Systems 70). As an illustration, the line $H_w(\nu)$ corresponds to the Fourier transform of a filter function $h_w(x)$ and is the transfer function of the first stage of image filtering being considered here.

In the absence of collimator penetration, and with perfect rejection of scattered gamma rays at the detector, $H_w(\nu)$ would be the MTF of the camera, except in the case of imaging with positron emitting isotopes. In the case of positron emission, the effect of the finite positron range before annihilation and emission of the 511 KeV photons can also be represented as one stage of image filtering. Positron emitting isotopes are not monoenergetic but emit positrons with energies up to a maximum, E_{max}, characteristic of the isotope. The Fermi theory of β-decay, with an approximation valid for nuclides with low atomic number[8], shows that the fraction of nuclei which disintegrate per unit time by emitting a β particle (electron or positron) with kinetic energy between E and E+dE is given by

$$P(E)dE = K(E+m_oc^2)\ (E^2+2\ m_oc^2E)^{1/2}(E_{max}-E)^2dE \qquad (3)$$

where m_oc^2 is the rest energy of an electron. With K chosen such that

$$\int_0^{E_{max}} P(E)dE = 1 \qquad (4)$$

the function P(E) acquires the character of a probability density function.

The range of a positron with initial energy E has often been calculated by integrating the reciprocal of the total stopping power

$$R(E) = \int_0^E \left[-\frac{1}{\rho}\left(\frac{dE}{dx}\right)\right]^{-1} dE \qquad (5)$$

where ρ is the density of the material through which the positron travels and (dE/dx) is the total energy loss per unit path length. Calculations for a large number of materials and initial positron energies were carried out by Berger and Seltzer[9] and results given in the form of tables for discrete values of E. Initial experiments on positron image degradation carried out by the authors based on the use of Eq. (5)[10] have shown that R(E) is not equivalent to the penetration depth in the initial direction of positron travel, but can best be described as a "path length". One can, however, postulate the existence of a function R(E), so that the probability

density function P(E)dE of Eq. (3) can be converted to a new density function P(R)dR, corresponding to the probability that a positron emitted by a particular nuclide will have a range between R and R + dR:

$$P(E)dE = \left\{P[E(R)] \frac{dE}{dR}\right\} dR = P(R)dR \qquad (6)$$

From the point of view of image formation, a point source of positrons can be viewed as the projection of P(R) on a plane parallel to the collimator face. This projection can be obtained from the spherically symmetrical function P(R) by the transformation

$$f_R(r)\ rdrd\theta = \int_{z=0}^{z'} P\left\{(r^2 + z^2)^{1/2}\right\} rdrd\theta dz, \qquad (7)$$

where $z' = (R_{max}^2 - r^2)^{1/2}$ and $f_R(r)$ is the desired projection.

The function $f_R(r)$ is then the response of a positron emitting system to a point source. Carrying out a Hankel transform on $f_R(r)$

$$F_R(\nu) = 2\pi \int_0^{\infty} r f_R(r) J_o(2\pi\nu r) dr, \qquad (8)$$

where J_o is Bessel's function of zero order, leads us to $F_R(\nu)$, the filter transfer function for the one-dimensional variations considered here.[11] This second stage of image filtering, for positron emitting isotopes only, is also represented schematically in Fig. 1. The MTF for a hypothetical camera without collimator penetration and perfect scatter rejection for positron emitting isotopes would be given by the product of $F_R(\nu)$ and $H_w(\nu)$ in Fig. 1. $F_R(\nu)$ can be obtained experimentally by comparing camera MTFs of two isotopes producing photons of similar energies with one of them being a positron emitter. This has been done and is reported below.

Collimator penetration and imperfect scatter rejection, although of distinct origin, can be treated together in a simplified practical approach. A calculation from first principles is quite complex and not justifiable for the purposes of the present work. It is convenient mathematically to divide the effects of penetration and scattering into two parts: near neighbors, and long range. Figure 2 shows conceptually this distinction. Long range effects have been found by our and other workers experience[1] to generate long tails in line response functions (LRF). These tails decay approximately linearly with distance from the source and therefore can be represented by a triangle with area A_p (fraction of total area under LRF) and a zero crossing at some point $x = \pm x_1$. Near neighbor effects can be characterized by coefficients C_1, C_2, C_3 ... corresponding to the count rate caused by penetration and scattering at detector elements or collimator holes neighboring the center element, whose response is C_0, after subtracting the triangular portion.

For a LRF normalized to unity area, the Fourier transform of these two parts can be easily calculated separately for near neighbor and long range effects. The transform of a symmetric triangle of base $2x_1$ and area A_p is

$$A_p\ [\text{sinc}\ (x_1\nu)]^2 \qquad (9)$$

The image reconstructed from the coefficients C_n by Eq. (1) is

$$\sum_{n=-\infty}^{\infty} C_n \left[\text{sinc}\ 2\nu_c \left(x - \frac{n}{2\nu_c}\right)\right]$$

which transforms into the series

$$\frac{1}{2\nu_c} R(2\nu_c)\left[C_o + \sum_{n=1}^{\infty} 2C \cos\left(\frac{n\pi\nu}{\nu_c}\right)\right] \qquad (10)$$

where $R(2\nu_c)$ is a rectangle function of unity height and extending from $-\nu_c$ to $+\nu_c$.

If the coefficients C_n could be calculated from first principles, the sum of expressions (9) and (10), (multiplied by $H_w(\nu)$ and $F_R(\nu)$ where applicable) would give the MTF of the collimator detector system for multi-crystal camera heads. For Anger type cameras, the intrinsic resolution MTF of the detector would have to be included also. In a practical situation, however, the LRF of a camera with a particular isotope, collimator, etc., can be measured and the MTF can be calculated from the sum of expressions (9) and (10) with the experimentally determined coefficients C_n. These also take into account the effects due to positron range where applicable, and hole averaging. Fig. 1 shows schematically the sections of the MTF shapes controlled principally by short and long range penetration and scattering effects. The initial drop in the MTF at low values of ν corresponds to the fractional area A_p of the long range tail. The rapid drop stops at the first zero of the $(\text{sinc}\ x_1\nu)^2$ function, at $\nu = 1/x_1$, at which point the MTF has a value of $(1-A_p)$.

Figure 3 shows a comparison of the MTFs calculated by Fourier transforming the experimental data and by using expressions (9) and (10) on the LRF of a Baird Atomic System 70 camera. Parameters for the measurement will be discussed in detail below. As expected, the agreement is quite good.

To summarize the ideas presented in this section, it can be stated that for a multi-hole, parallel-wall collimator:

a) The distance between holes, d_s, determines a maximum usable frequency $\nu_c = 1/2d_s$.

b) Collimator hole geometry determines the maximum values of MTF that the collimator can allow, given by a function $H_w(\nu)$ valid to $\nu = \nu_c$.

c) Positron range can limit that maximum MTF to the product $H_w(\nu) \cdot F_R(\nu)$.

d) Long tails in the LRF result in a sharp decrease in MTF values, reducing contrast at all but the lowest frequencies by the fractional area under the tail.

e) Near neighbor penetration and scatter have an effect primarily on the shapes of the MTF at the middle and higher frequency end.

f) The MTF of multi-crystal detector heads can apparently be better than for Anger type cameras, since the intrinsic detector MTF is unity up to ν_c.

SINGLE ELEMENT GERMANIUM CAMERA EXPERIMENTS

A coaxial Ge(Li) detector of 20 cm^3 volume has been used as a "one-element" camera by fitting it with appropriate shielding and with a collimator of variable length. Figure 4a shows schematically the setup used for the measurements. The distance between the line source and collimator face was variable and the line could be displaced vertically with respect to the collimator aperture. Another detector, made of high-purity germanium, with a volume of approximately 8 cm^3 and a cross-sectional area of 7 cm^2, was used for the positron range measurements. Resolution of the Ge(Li) system was approximately 3 keV FWHM at 122 keV, while the second system operated with a figure of 1.0 keV FWHM at the same energy.

Maximum Collimator Resolution

As discussed above, the maximum collimator MTF can be represented by a function $H_w(\nu)$ which is the transform of a weighting function $h_w(x)$. $H_w(\nu)$ is valid only up to a frequency $\nu_c = 1/2d_s$, where d_s is the distance between adjacent holes. The collimator for the one-element germanium camera had only one aperture, so that ν_c is not defined strictly. For an aperture of dimension d in the direction of motion of the line source and infinite thickness, the closest spacing without overlap between sampling positions is also d, as in the Baird Atomic System 70 camera, so that one can specify ν_c as being 1/2d.

The function $h_w(x)$ can be obtained by a simple geometrical construction as indicated in Fig. 4b. For $-b \leq x \leq b$, the response of the detector to a line source at x will be practically constant. For $b \leq |x| \leq B$, a linear decrease in response should be sufficiently correct. With the flat top at unity

$$h_w(x) = \frac{B}{B-b}\ T\ (2B) - \frac{b}{B-b}\ T\ (2b) \qquad (11)$$

where T(2m) stands for a trianglular function of base 2m and unity height. The corresponding normalized $H_w(\nu)$ is then

$$H_w(\nu) = [B(\text{sinc } B\nu)^2 - b(\text{sinc } b\nu)^2]/(B-b) \qquad (12)$$

The parameter B can be obtained from geometrical relationships as $B = b(2z + L)/L$ with the parameters defined in Fig. 4b and $b = d/2$. The resulting functions, $H_w(\nu)$ for several values of d, t, and z, to be used in the experiments below, are shown in Fig. 5a. The cutoff frequencies are also shown. The effect of using tapered holes with equal aperture at the detector as in the parallel-hole case, has been investigated. Substantial improvement in the geometric MTF can be obtained by using tapered holes with a focal distance s of magnitude similar to the source-to-detector distance (L + z). Figure 5b shows some of the results obtained. With d being the aperture at the detector end, it is found that $b = 0.5\ d|1-(L+z/s)|$ and $B = b + (dz/L)$. Equation (12) can then be used.

It must be realized that this geometric or point averaging MTF assumes no penetration by radiation. Practically, this will be true only for low energy isotopes.

Effects Due To Positron Range

When positron emitting isotopes are used for imaging, a second step of filtering can be considered to exist in the imaging system, as indicated in the theoretical analysis given above. The probabilities that positrons will be emitted with energy between E and (E + dE) from four of the more interesting positron emitting isotopes (^{18}F, ^{11}C, ^{13}N and ^{15}O) have been calculated from Eq. (3) and the results are shown in Fig. 6a. If the assumption is made that only small angle scattering occurs until the positron energy is quite small, i.e., that it is reasonable to assume that positron "path length" and range in the initial direction of travel are approximately equal, one can use the range-energy data of Ref. 9 for water and obtain the probability that an emitted positron will have a range between R and (R + dR). The transformation indicated by Eq. (6) accomplishes that goal. The function $f_R(r)$, the projection of P(R), can then be obtained by the use of Eq. (7). The results are shown in Fig. 6b. Finally, a Hankel transform leads to $F_R(\nu)$, the filter function for variation in one direction, shown in Fig. 6c. In order to test the validity of these calculations, careful measurements of the MTF of a Nuclear Chicago HP camera equipped with a pinhole collimator and a Medi-Physics insert with an aperture of 0.9 cm were made. A comparison between the MTFs obtained from a line immersed in water and filled successively with ^{85}Sr (514 keV) and the four positron emitters studied failed to show any differences, although some would have been observed if the results of Fig. 6c were correct. This finding suggests that the range is not as long as the "path length" obtained from Ref. 9.

A second set of measurements with a germanium detector in the arrangement described by Fig. 4 was made. A collimator of dimensions d = 0.2 cm, L = 15 cm, a distance z = 1.25 cm, and a line of diameter 1 mm embedded in plastic ("Lucite") were used. The thickness of plastic on either side of the line was 1.25 cm. Figure 7 shows the functions $F_R(\nu)$ obtained for the positron emitters by dividing the MTFs measured with them by the MTF obtained from ^{85}Sr. The data obtained are of limited validity at the high frequency end. The difficulty in obtaining good statistics with the short-lived isotopes and the low specific activity ^{85}Sr isotope in soluble form, and the use of a very sharp collimator, translates itself into invalid high frequency information in the transformation of the measured LRFs. The lines presented in Fig. 7 are, therefore, incomplete at the high frequency end and cannot be used properly to work back into obtaining a correct experimental range-energy relationship to replace the simplified relationship of Eq. (5).

A comparison of the results of Fig. 7 and 6c shows that, as expected after the first set of measurements with a commercial camera, the adverse filtering action due to positron range is not as severe as predicted by the simple relationship of Eq. (5). If very sharp positron cameras are constructed, however, a substantial MTF limitation will exist, particularly with the very short-lived ^{15}O. On the other hand, work with ^{18}F is very unlikely to be affected by positron range effects in normal tissue even with very sharp cameras which exist now only in concept.

Effects Due To Penetration And Energy Resolution

Measurements of the LRF were also carried out using a single element Ge system in the configuration of Fig. 4 with the window of a single channel analyzer (SCA) set at ± 2.4 keV about the approximate center of the photoelectric peak of the isotopes studied. Measurements were made with the line at distances z = 2.1 and 7.3 cm from the collimator. The line was sandwiched between two plates of tissue equivalent rubber material, each with a thickness of 1 cm. The results of those two measurements should show the effect of collimator geometry averaging. Next, the absorber thickness at the detector wall was increased to 5 cm without changing the value of z = 7.3 cm. The effect of the radiation scattered by the absorber should then have become noticeable. The window setting of the SCA was also changed to simulate the effects of a detector with poor energy resolution. Spectra from a pulse height analyzer were taken at points where they could help in understanding the origin of the counts registered by the detector as the line was swept past the collimator aperture at increments of 1 mm per point.

The LRF and MTF results obtained with technetium-99 m are shown in Fig. 8. A comparison of the MTF lines for a thin absorber (a = 1 cm), labeled 1 and 2, with the corresponding calculated lines of Fig. 5a, shows good agreement although the experimental results are somewhat better. This is probably due to the two sections of the collimator (5 cm each) not being perfectly well aligned in the experiment. The presence of the thick absorber is noticeable in the MTF when the window (W) was ± 2.4 keV. Opening the window of the SCA results in the appearance of tails in the LRF and a consequent initial drop of the MTF. A window of ± 14 keV was intended to simulate the effect of using a fairly well coupled NaI(Tl)-photomultiplier combination; a indow of ± 35 simulates the use of that same detector combination with coupling by long light pipes.

Energy spectra obtained at positions A, B, and C indicated in Fig. 8a, and corresponding to the line being positioned at the center of the collimator aperture, at 0.4 cm, and at 0.9 cm from the center, respectively, are shown in Fig. 9a, b and c. The windows used in the experiments are shown by the position of the Lower Level Discriminator of the SCA. The thick absorber was present. Examination of the results shows that even with W = ± 2.4 keV a substantial amount of scattering is being accepted at positions B and C, giving rise to some tails in the LRF. With the larger value of W it is very clear that scattering is the cause of the observed tails.

The results obtained with ^{18}F at 511 keV are shown in Fig. 10. With W = ± 2.4 keV, a small tail, independent of position or absorber thickness, is apparent and the introduction of the thick absorber is practically unnoticeable. Opening W to ± 127 keV results in a substantial increase in the tail and the corresponding change in the MTF. The relative insensitivity of the MTF to energy resolution at 511 keV is consistent with the results of a simplified evaluation carried out previously[12] and the conclusions arrived at in that study are supported by present findings: One does not need the energy resolution of germanium in cameras for positron emitters, but a moderate amount of resolution is still required. The degradation in MTF due to opening W to ± 127 keV is not insignificant in low contrast imaging situations as will be discussed below.

Figures 11a, b, c and d show the spectra obtained at positions A, B, C, and D of Fig. 10a. The presence of a photopeak even in position D is quite evident, indicating that 10 cm of lead are not enough to prevent some penetration, as indeed a straight forward calculation shows. Opening the window again shows how the acceptance of scattered radiation results in image degradation.

The results of the experiments with the single element germanium camera can be summarized as follows:

a) With sufficiently deep collimators to minimize penetration and with the good energy resolution of germanium detectors, the system MTF can be expected to follow Eq. (12), (the filtering due to averaging at each sampling point) depending exclusively on collimator geometry. The upper frequency cutoff is then determined by the sampling distance.

b) Positron range effects in water with cameras showing little response above $\nu = 1\ cm^{-1}$ at 511 keV (presently available commercial cameras) are negligible. Their effects should be taken into consideration, however, in the design of higher resolution cameras, particularly for the higher positron energy emitting isotopes.

c) At energies in the vicinity of 140 keV, tails in the LRF are due to poor scatter rejection by the detector system, as long as the collimator thickness is sufficient to prevent direct penetration.

d) At energies in the vicinity of 511 keV, tails can be due to direct penetration through the collimator, even with thicknesses of 10 cm of solid lead.

e) Energy resolution affects MTF shapes quite substantially at the lower isotope energies, but much less at the higher ones. A relationship between MTF shape and imaging capabilities will be established in the section on "The MTF And Image Quality" below.

NaI(Tl)-PHOTOMULTIPLIER CAMERA STUDIES

In trying to establish the necessity for a camera with detectors of high energy resolution, it is necessary to carry out a comparison between the expectation for performance of such a camera and some well established presently available systems. For that purpose, measurements of the MTF under conditions similar to the ones used for the Ge experiments were carried out with two cameras of different basic designs: the Baird-Atomic System 70, with multiple crystals, and the Nuclear Chicago HP camera, of the Anger type. It must be clear that the value, quality, or capabilities of a camera cannot be determined solely from its static imaging characteristics, but it is also certain that in studying static imaging, the LRF-MTF method provides the simplest and potentially most complete information regarding the image-forming abilities of a gamma camera.

Multiple Crystal Camera

The three measurements of LRF described above for the Ge experiments were repeated with the System 70 camera using ^{99m}Tc and ^{18}F. With the 1 mm diameter line carefully positioned along one of the camera

axes and relatively well centered with the collimator holes at the initial scan position, the standard 16-position sequence was initiated. The 6.35 cm thick collimator was used. It has tapered holes of focal distance 10.8 cm. The data obtained were integrated over a length of line of 5.5 cm and read out at values of x in intervals of 0.277 cm (the sampling distance of the camera). The raw data for the LRF at small distances (z = 2.1 cm) appeared somewhat unsymmetrical, indicating imperfect positioning of the line. Although the computer program for MTF calculation performs a symmetrization before the Fourier transformation, some error in the results can be expected. For z = 7.3 cm the raw data were quite symmetrical, indicating that the positioning error was indeed small and was being smoothed out by the averaging function of the collimator at the larger distance. The errors caused by the finite dimensions of the line source have been investigated and found to be negligible for all the measurements reported in this paper. Finally, care has been taken so that the Fourier transform of a LRF with few data points in the more rapidly varying parts of the function can be obtained with accuracy. Integration programs assuming parabolas over three points are needed in order that a second transformation reproduces the original data with errors much smaller than the differences in the data for the three measurement conditions for each isotope.

Figure 12 shows the results obtained with ^{99m}Tc. A substantial tail in the LRF, even with 1 cm of absorber, was quite evident. The tail fractional area was $A_p \simeq 0.17$. With a 5 cm absorber A_p became approximately 0.45. The parameter x_1 of Eq. (9) was measured to be approximately 6.9 cm, and indeed the initial drop of the MTF stops at approximately $\nu \approx 1/x_1 = 0.14$ cm^{-1}. The value of $A_p \sim 0.45$ corresponds approximately to the size of the initial drop in MTF observed with Ge with a window W = ± 35 keV, which was $A_p \sim 0.38$, Fig. 8. Since the collimator is sufficiently thick that direct penetration is not possible at 140 KeV of energy, it is evident that the MTF drop at low ν is due to the energy resolution characteristics of the camera. The intrinsic maximum MTF due to the sampling distance and the collimator geometry MTF at z = 7.3 cm are also shown. They were calculated from Eq. (12) using the collimator parameters (d = 0.634, s = 10.8 and L = 6.35 cm). It becomes apparent that the high frequency response is limited by the collimator geometry. Although the sampling distance is 0.277 cm, the effective apertures of the collimator are substantially larger than this figure and a great deal of geometric overlap occurs. Smaller apertures or longer holes would improve the MTF, but at the expense of count rate efficiency.

Figure 13 shows the corresponding results for ^{18}F. A large tail, with $A_p \sim 0.52$ appears in the LRF even with an absorber thickness of (a = 1.0 cm). A_p increased to approximately 0.58 cm when a = 5 cm. It is evident that penetration through the 6.35 cm collimator is responsible for the large penetration fraction, since a 10 cm collimator still resulted in full energy photoelectric events at large values of x with the Ge detector. The additional increase in A_p when the 5 cm absorber was installed must then be due to the energy resolution characteristics of the system. Intrinsic and geometric MTFs at z = 7.3 cm are also included in the figure.

Anger-Type Camera

Experiments identical to the above ones were carried out with the Nuclear Chicago HP camera. X and Y position signals from the camera were processed through a level change and pulse shaping for acceptability to a 256 channel pulse-height analyzer. X signals originating over a length of line of 5 cm at the center of the camera were utilized. Data in the X-direction were taken at intervals of 0.12 cm and processed in the same computer programs as in the previous experiments. Intrinsic camera resolution measurements were made with a 60 cm line of 1 mm diameter inside the trough of a lead collimator of the same length and aperture, respectively, and a depth of 10 cm. Wall thickness was 5 cm. The energy window of the system was set at 20% for all the measurements.

Results obtained with ^{99m}Tc using the high resolution collimator made for that isotope by Nuclear Chicago are shown in Fig. 14. At a distance z = 2.1 cm the MTF results are practically indistinguishable from the intrinsic camera resolution, indicating a very good match of capabilities. Little degradation occurs at d = 7.3 cm or with the introduction of the thicker absorber. The principal limitation appears to be in the intrinsic MTF which, when multiplied by all the other filter functions, is a dominant factor.

The experiments with ^{18}F were carried out with two collimators: 1) a tungsten (W) collimator as designed by Harper, et al[13]; 2) pinhole collimator manufactured by Nuclear Chicago, fitted with a 0.9 cm diameter insert made by Medi-Physics for 511 KeV isotopes and with the addition of a 1.25 cm shield plate of lead around the collimator opening to decrease direct penetration. The intrinsic camera resolution at 511 KeV was found to be much better than for ^{99m}Tc, and neither of the two collimators tested does the detection system good justice.

The LRF of the W collimator shows a long tail with A_p between 0.05 and 0.10 and substantial near neighbors penetration. The shortest possible distance (the x-direction) between successive rows of holes is 0.735 cm, so that the theoretical cutoff frequency for this experiment is $\nu_c = 1/(2 \times 0.735) = 0.68$ cm^{-1}. The ratio of C_1/C_0, as in Eq. (10), for position 1 at x = 0.735, is approximately 0.21. These factors, plus a relatively large hole diameter (0.61 cm) reduce the collimator MTF quite strongly.

The pinhole collimator at 1:1 magnification showed poorer results than the W collimator. It is also evident from Fig. 15 that the camera resolution is quite insensitive to the presence of scattered radiation.

Conclusions from the studies with these two camera systems in the context of the subject matter of this research will be drawn in the final section of the paper.

THE MTF AND IMAGE QUALITY

A study based on comparison of the MTFs of different systems is quite objective but does not readily allow an assessment of what actual images will look like in a clinical situation. For the purposes of the present work it was clearly necessary to establish whether a certain drop in MTF due to poor energy resolution in a system is significant in terms of the ability to form an image of an isotope distribution. In a high constrast imaging situation, like simple bar phantom studies, or hot spots in cool

fields, the effect of decreases in the MTF may be of little consequence if one can subtract a uniform number of counts from the whole field of the image and thus increase contrast. In low contrast situations, and in particular in attempting to detect somewhat cooler spots in hot areas, one may need as much contrast as possible and, correspondingly, the best scatter rejection.

In order to obtain a semi-quantitative understanding of the relationship between MTF and imaging, a two dimensional, circularly symmetrical phantom was generated by computer and the images that a camera with a particular MTF would generate were obtained. A "difficult" pattern was used for those simulations: A circle with 100% activity, of 9 cm diameter with a smaller circle of 1.0 or 0.5 cm diameter of 70% activity. By using camera MTFs obtained from actual measurements with a 5 cm absorber, this flat pattern appeared, in effect, to have been placed under a 5 cm absorber, so that radiation from the hotter zone found a substantial amount of scattering material between the cool zone and the collimator. The two test patterns are shown in Fig. 16a. The source distribution s(r) is Hankel transformed to a circularly symmetrical $S(\nu_r)$, shown for the 1 cm diameter cool spot case in Fig. 16b. This function was then multiplied by the MTF of a particular camera and the result again Hankel transformed to obtain a reproduction of S(r) after passing through the camera. Figure 16b shows the MTF of a hypothetical "super camera" with a value of near unity up to $\nu = 2.5$ cm^{-1}, and Fig. 16c shows the two images generated by such a camera. The images were formed by extending the reproduced s(r) in a 64 x 64 matrix, normalizing the number of count of each cell to a predetermined total number of counts and then applying a Poisson type noise to each cell with a standard deviation $\sigma = \sqrt{N}$, where N was the original number of counts in the cell. It was found that 400,000 counts over the complete field were needed in order to be able to see the 0.5 cm cool zone unequivocally. An identical number of total counts were used for all the images. The oscilloscope contrast was set in a position so that 70% activity looked black, and all settings were identical in all the pictures. Also, in all cases the MTFs obtained at z = 7.3 cm and with the 5 cm absorber in place were used.

Figure 17 shows the results obtained from the Ge single element camera for ^{99m}Tc at three settings of the energy window. The MTFs that generated the images are shown at the top of the figure. A setting of W = ± 14 KeV does not result in a very substantial degradation, although W = ± 35 KeV is definitely damaging to the image. The Ge camera was also tested with a narrower, longer collimator (0.2 x 15 cm) in order to ascertain whether a camera with very high collimator resolution could make good use of the energy resolution of germanium. Figure 18 shows the results obtained. The images for W = ± 14 KeV in Figs. 17 and 18 are very similar, but the images for W = ± 2.4 KeV with the finer collimator, Fig. 18, are substantially better than those of Fig. 17, particularly in the case of the 0.5 cm cool spot. This finding is quite similar to the results obtained in the analysis of scanners, Ref. 1., i.e., good energy resolution is a requirement only when fine imaging is desired. Present simulations show that germanium can be used to advantage when the collimator MTF is good enough to have substantial values above ν = 2 cm^{-1}. Otherwise, optimally coupled NaI(Tl)-photomultiplier systems may be adequate.

The results with germanium at 511 KeV are shown in Fig. 19. When W = ± 2.4 KeV the results are almost as good as those obtained at 140 KeV. Opening the window to W = ± 127 KeV is almost as bad as it was to open W to ± 35 KeV at the ^{99m}Tc energy, indicating that good NaI(Tl)-photomultiplier coupling is still a requirement for positron emitter imaging of low contrast situations.

Use of the MTFs of the two camera systems studied produced considerably poorer images. Figures 20 and 21 show the reconstructed images. It appears empirically true, and it is theoretically reasonable, that in order to clearly see objects of diameter d in low contrast situations it is necessary to have a MTF with substantial values (0.4 to 0.5) up to $\nu = 1/d$. Better collimation would have allowed the two cameras to see the phantom much better up to the limited imposed by their energy resolution, but considerations of efficiency in relation to radioisotope dose and patient imaging time have to be taken into account in the design of a camera. This point will be considered next.

EFFECT OF COUNTING STATISTICS

In this section, the number of counts per unit area required to obtain an image of the kind presented in the previous section will be investigated as a function of the size of the "cool" spot. A relationship between efficiency and imaging capabilities will then be obtained in order to estimate the clinical usefulness of a high resolution camera.

For a similar situation with rectilinear scanners,[1] it was found that the relationship between the required count rate and the standard deviation of Gaussian filters to obtain equal amounts of noise is given by

$$\frac{\bar{N}_1}{\bar{N}_2} = \frac{\sigma_{f_2}}{\sigma_{f_1}} \qquad (13)$$

where N_1 and N_2 are count rates and their respective standard variations are σ_{f_1} and σ_{f_2}. The standard deviations in the frequency domain of the Gaussian filter are $1/2\pi\sigma_{f_1}$ and $1/2\pi\sigma_{f_2}$.

Consider two images of the same subject obtained by two cameras with arbitrary cutoffs of their MTFs (e.g. at 10%) defined by ν_{c_1} and ν_{c_2}. In order to do good filtering in both cases, one could choose a Gaussian filter with a standard deviation $K\nu_c$, with K of the order of 1. With this choice of filtering, we obtain from Eq. (13)

$$\frac{\bar{N}_1}{\bar{N}_2} = \frac{\nu_{c_1}}{\nu_{c_2}} \qquad (14)$$

This means that in order to do the best job of extracting information by filtering both images, leaving the same amount of "hash" in both cases, the count rates will have to be proportional to the frequency cutoff of the camera.

From the previous observation that in order to see a cool spot of diameter d_s in a much larger hot field, the camera MTF must be substantial (e.g., 0.4 to 0.5) at a frequency $\nu = 1/d_s$, one can set the

requirement that $\nu_c \propto 1/d_s$ and Eq. (14) becomes

$$\frac{\bar{N}_1}{\bar{N}_2} = \frac{d_{s_2}}{d_{s_1}} \qquad (15)$$

i.e., that the number of counts required per unit area is inversely proportional to the size of the cool spot to be observed.

The time required to obtain a certain number of counts from a collimator can be calculated most easily for square holes, but the results should be of general applicability. In the section "Maximum Collimator Resolution", the weighting function caused by the field of view of one collimator hole was described in terms of parameters b and B of Fig. 4. With variations in two dimensions, the volume of such weighting functions will be proportional to the count rates at the detector end for a fixed source at a distance z. These relative volumes are given by

$$V = \frac{4}{3} \frac{B^3 - b^3}{B - b} \qquad (16)$$

If one takes as reference the Baird-Atomic System 70 camera with the 6.35 cm collimator with an efficiency which appears to be quite acceptable in clinical practice and assigns a hole speed coefficient of unity to the geometry of an individual hole (which is scanned over 16 positions to obtain an image), one can calculate the speed coefficients of cameras of similar basic construction, but with finer collimation. If one could pack more crystals per unit area, the camera speed factor would increase proportionally as fewer scanning positions would be needed. Also, a factor corresponding to the photopeak detection efficiency has to be included in an overall efficiency calculation.

By using the relationship described above between collimator MTF and the size of a cool field which can be seen in a low contrast situation, it is found that the speed coefficient is very insensitive (for a fixed distance z) to the actual design parameters of a collimator, as long as a certain MTF is obtained, so that it is possible to show such a relationship in one single graph. Figure 22 shows the results obtained for z = 7.3 cm.

According to the criterion adopted, the reference System 70 collimator would distinguish well a 70% activity of 1.85 cm diameter in a large field of 100% activity (collimator MTF = 0.45 at ν = 0.54). To see a 0.5 cm diameter cool field with a much finer collimator would require approximately 15 times more counting time from an identical source due to the smaller field of view of each collimator hole (speed coefficient of 1/15, from Fig. 22). If it were possible to pack a four times greater number of detectors per unit area than in the System 70 camera, the imaging time required would be approximately 3.75 times larger (for detectors of the same efficiency as those of the System 70 camera). This is the increase in counting time required to obtain the same number of counts from a fine collimator as would be obtained from the System 70 collimator. But, as was derived above, for fine imaging, it is also necessary to accumulate more counts. From Eq. (15), a factor of 1.85/0.5 in the number of counts/cm^2 is required for the production of a statistically clean image of a cool spot of 0.5 cm diameter. Then, the overall counting time requirements increase by a factor of 15 x 3.7 = 55.5 for a detector packing density similar to the S-70 System, or 14 times if one can pack four detector elements in the same area now occupied by one element in that camera.

To complete this feasibility analysis, the detector photoelectric efficiency should be considered. This can be done by using the product of detector efficiency and packing density instead of the simple packing density used above.

DETECTOR EFFICIENCY

The calculation of detection efficiency for the discrete detector case, which is being emphasized in this paper because it is a configuration which can be implemented with semiconductor detectors, can be carried out in an approximate, but useful form, by considering contributions to the photopeak signal coming only from a direct photoelectric event or from a Compton scattering event followed by a photoelectric event. For small detectors this would give a lower bound to efficiency. By adding the possibility of two consecutive Compton interactions and assuming that after such a process the gamma ray still gets collected at the detector an upper bound to efficiency can be obtained. A detailed description of the calculation procedure can be found in Ref. 12.

For cylindrical detector elements of a given diameter and length, the photopeak efficiency bounds have been calculated for gamma rays of 140 and 511 keV incident normally at the center of the circular entrance face and are shown in Fig. 23. Available materials (NaI(Tl), Ge) and possible alternative ones (CdTe and HgI_2) were considered. Some of the lengths used may be totally impossible to implement at present, although germanium detectors can be made with the field perpendicular to the direction of the incident gamma ray. The error bars in the graphs indicate upper and lower bounds for efficiency.

As a reference for comparisons, NaI(Tl) crystals with dimensions similar to the ones used by the Baird-Atomic System 70 will be considered, assuming a circular cross section equal to the area of the Systems 70 crystals. This corresponds to a diameter of 0.89 cm and a length of 3.8 cm. From Fig. 23a the photopeak efficiency $\varepsilon_{140} \simeq 0.9$ at 140 keV and $\varepsilon_{511} \simeq 0.3$ at 511 keV. The packing density is 0.82 detector per cm^2.

The first material to be considered for a possible high resolution camera is germanium. Since this material has a photoelectric attenuation coefficient at 140 keV which is of the same order as the Compton coefficient, the assymptotic efficiency for long, thin crystals at 140 keV is approximately 0.5. Only by increased diameter can one obtain higher photoelectric efficiencies. At 511 keV Compton interactions are dominant and crystal volume is of primary importance.

In order to increase the packing density of germanium detectors for the purpose of reducing the times required to form images at higher resolution, we shall consider using four detectors per cm^2 with an effective diameter of 0.4 cm (they could be of square cross section). From Fig. 23b it is evident that an efficiency at 140 keV of between 0.5 and 0.6 is feasible with elements of 2 to 3 cm length. The product of photopeak efficiency times packing density is approximately 2.2 vs 0.74 for the System 70 camera, a factor of three better. Camera designs with crossed bar patterns on a wafer can have higher

density in principle, may be 9 elements per cm^2, and for a wafer thickness of 1.0 cm this would give a photopeak efficiency times packing product of approximately 3.5, a factor of 4.7 better than in the System 70 camera.

A variation in design that is quite conceivable is the use of the "Compton Energy Sum" described in Ref. 12, by which one accepts the Compton scattered counts from a small detector if the detected energy added to the signal of a large germanium detector placed immediately behind the array adds up to the full energy of the isotope. An estimate of the efficiency of such a system results in a figure of 0.60 at 140 keV for the 0.2 x 1 cm detectors, nearly a factor of two improvement, but at a substantial cost.

CdTe shows higher efficiency than Ge and NaI(Tl) and can be operated at room temperature. Materials development programs should be watched to see if good energy resolution at 140 and 511 KeV is attainable with crystals of that material of 0.5 to 1 cm thickness on a routine basis. Counts appearing in low energy tails due to trapping, contact effects, etc. should not occur, as they detract from the photopeak efficiency.

A newer material, HgI_2, with high efficiency at 140 KeV has shown very interesting results to date,[14,15] and appears promising for use in high resolution cameras at the lower energies. From Fig. 23d it is evident that 1.5 mm thick crystals, with an efficiency $\varepsilon_{140} \simeq 0.7$ per crystal, could be packed quite closely since the photoelectric cross sections dominates over Compton effects very strongly and, therefore, crystal diameter is immaterial. The material suffers at this time from strong hole trapping but work is in progress to improve detector characteristics.

None of the detector materials studied are very efficient at 511 KeV. This fact, plus the possibility of avoiding collimators by using the time coincidence of the two annihilation photons from positron emitting isotopes places the design of optimal cameras for that energy in a different category. Reference 12 presents a study of the capabilities of solid state detectors for positron cameras. Successful design of a high resolution camera for 140 KeV would, however, represent an advance at 511 KeV, although long solid collimators would have to replace spaced collimating plates which could be used at the lower energies.

CONCLUSION

In this rather length study of gamma cameras, it is hoped that the following has been accomplished:

1) The different elements which affect image resolution have been separated and their individual effects on system MTF have been demonstrated.

2) It has been shown that energy resolution is of importance in imaging low contrast isotope distributions, particularly with isotopes emitting relatively low gamma energies. As an example, it has been demonstrated that when a cool spot of dimensions of the order of 0.5 cm has to be viewed in the presence of a large hot field at 140 KeV the energy resolution of germanium detectors becomes necessary. This performance requires, however, the use of sharper collimators than those used in clinical practice at present.

3) Presently available commercial gamma cameras fail to image such low contrast isotope distributions due either to limitations in the intrinsic camera resolution (HP) or to collimator-energy resolution characteristics (S-70). Cameras with discrete NaI(Tl) detector elements and better collimators could perform much better than present ones, without much loss in speed, by packing more detectors per unit area, provided that energy resolution could be kept to about 15 KeV FWHM for 140 KeV gammas. Since this latter condition is not likely to be met with NaI due to light piping losses, it appears that germanium cameras with small elements, closely packed, is the only way to improve imaging of low (and obviously also high) contrast distributions.

3) Germanium, and other semiconductors possibly available in the future, open up, therefore, the capabilities for higher resolution imaging in comparison with presently available systems. However, a penalty is paid in the time needed to form a statistically meaningful image. For example, viewing with ^{99m}Tc and a germanium camera the cool spot indicated above would take roughly 14 times longer than the time required to observe a 1.85 cm cool spot with the System 70 camera. By use of the "Compton Energy Sum" method this time could possibly be reduced by a factor of two.

4) The camera design parameters for effective use of high resolution detectors have been presented in terms of relationships to system MTF and efficiences.

It is felt by the authors that the desire for better images in Nuclear Medicine is a strong one. It is less clear, however, to what extent clinical practice and/or medical research would use improved imaging if faced with increased imaging time. The authors would like to express the opinion shared by many in the field, that the answer to this question can only come from actual medical experience with a well designed and constructed camera of useful dimensions, and with a set of collimators that allows it to function at different efficiences and resolutions.

ACKNOWLEDGMENTS

The authors would like to acknowledge the cooperation of Jan Siemsen, for help with camera measurements, the assistance of the Staff of the Medical Cyclotron, UCLA, for providing positron emitting isotopes, the interest and support of Gerald C. Huth, and the assistance of Carl Selin, with the computer image simulations. Numerous discussions with members of the Nuclear Medicine Research Labs and Clinic, UCLA, are gratefully acknowledged. The authors are indebted to Fred S. Goulding, Lawrence Berkeley Laboratory, for his comments and interest on this paper and for committing his resources in preparing the work for publication.

REFERENCES

1. R. N. Beck, M. W. Schuh, T. D. Cohen and N. Lembares, Medical Radioisotope Scintigraphy, Volume I, Proceedings of a Symposium, I.A.E.A., 595 (August 1968).
2. J. Llacer, IEEE Trans. Nucl. Sci., NS-20, No. 1, 273 (1973).
3. R. P. Parker, E. M. Gunnersen, J. L. Wankling and R. Ellis, Med. Rad. Scintigraphy, Proc. of a Symposium, I.A.E.A., 1, 71 (1968).

4. M. G. Strauss and I. S. Sherman, IEEE Trans. Nucl. Sci., NS-19, No. 3, 219 (1972).

5. J. E. Detko, Radiology, 104, 431 (1972).

6. L. Kaufman, G. A. Armantrout, D. C. Camp, J. H. McQuaid, S. P. Swierkowski and K. Lee, IEEE Trans. Nucl. Sci., NS-21, No. 1, 652 (1974).

7. P. A. Schlosser, D. W. Miller, M. S. Gerber, R. F. Redmond, J. W. Harpster, W. J. Collis and W. W. Hunter, IEEE Trans., Nucl. Sci., NS-21, No. 1, 658 (1974).

8. K. Siegbahn, Beta And Gamma-Ray Spectroscopy, North Holland, 33 (1955).

9. M. J. Berger, and S. M. Seltzer, Tables of Energy Losses and Ranges of Electrons and Positrons, NASA SP-3012.

10. L. S. Graham, N. S. MacDonald, G. D. Robinson and J. Llacer, J. Nucl. Med., 14, 401 (1973).

11. R. M. Beck, C. T. Zimmer, P. B. Charleston, F. V. Harper, and P. B. Hoffer, Medical Radioisotope Scintigraphy, Proceedings of a Symposium, I.A.E.A., Vienna, 1, 3 (1973).

12. J. Llacer and Z. H. Cho, IEEE Trans. Nucl. Sci., NS-20, No. 1, 282 (1973).

13. P. V. Harper, et al., Radiology, 108, 613 (1973).

14. S. P. Swierkowski, G. A. Armantrout and R.Wichner, IEEE Trans. Nucl. Sci., NS-21, No. 1, 302 (1974).

15. J. Llacer, M. Watt, M. Schieber, R. Carlston and W. Schnepple, IEEE Trans. Nucl. Sci. NS-21, No. 1, 305 (1974).

FIGURE CAPTIONS

Fig. 1. Conceptual description of factors affecting the shape of the Modulation Transfer Function (MTF) of a camera.

Fig. 2. Conceptual description of factors affecting the shape of the Line Response Function (LRF) of a camera.

Fig. 3. Comparison between MTFs computed by direct Fourier transformation of two experimental LRFs and by separate term Fourier transforms. (Equations (9) and (10).)

Fig. 4. a) Schematic representation of experimental setup with germanium detector,

b) Geometrical construction of $h_w(x)$ for parallel hole collimators.

Fig. 5. a) Filter function $H_w(\nu)$ for several parallel hole collimator dimensions.

b) Showing effect on $H_w(\nu)$ of using tapered holes of focal distance s.

Fig. 6. a) Probability distribution of positron energies for four radioisotopes of interest (from Fermi theory).

b) Projection into a plane of probability distribution of positron ranges, assuming that "path length" and range in direction of initial travel are equivalent.

c) Filtering functions due to positron range with the above assumption.

Fig. 7. Filtering functions due to positron range obtained by measurement. Comparison with Fig. 6c indicates that "path length" and range are not equivalent.

Fig. 8. LRFs and MTFs for single element germanium camera showing collimator and-energy resolution effects for ^{99m}Tc isotope.

Fig. 9. Energy spectrum of germanium detector with line source in positions A, B and C of Fig. 8a, ^{99m}Tc isotope.

Fig. 10. LRFs and MTFs for single element germanium camera showing collimator and energy resolution effects for ^{18}F isotope.

Fig. 11. Energy spectrum of germanium detector with line source in positions A, B, C and D of Fig. 10a, ^{18}F isotope.

Fig. 12. LRFs and MTFs for Baird Atomic System 70 Camera, ^{99m}Tc isotope.

Fig. 13. LRFs and MTFs for Baird Atomic System 70 Camera, ^{18}F isotope.

Fig. 14. LRFs and MTFs for Nuclear Chicago HP Camera, ^{99m}Tc isotope.

Fig. 15. LRFs and MTFs for Nuclear Chicago HP Camera, ^{18}F isotope.

Fig. 16. a) Activity distribution functions for low contrast flat circularly symmetric phantoms.

b) Hankel transform of the left test pattern and MTF of a hypothetical "supercamera".

c) Reproduction of test patterns by "supercamera" with 400,000 counts in the complete image.

Fig. 17. Reproduction of test patterns by hypothetical germanium camera as a function of the energy resolution window setting, with 5 cm absorber between source and camera, ^{99m}Tc isotope.

Fig. 18. Reproduction of test patterns by hypothetical germanium camera with very long collimator, ^{99m}Tc isotope, 5 cm absorber.

Fig. 19. Reproduction of test patterns by hypothetical germanium camera, ^{18}F isotope, 5 cm absorber.

Fig. 20. Reproduction of test patterns by S-70 camera, ^{99m}Tc and ^{18}F isotopes, 5 cm absorber.

Fig. 21. Reproduction of test pattern by HP camera, ^{99m}Tc and ^{18}F isotopes, 5 cm absorber.

Fig. 22. Speed coefficient of camera collimators as a function of cool spot diameter visible in low contrast situation, relative to the S-70 collimator system.

Fig. 23. Photopeak detector efficiencies for NaI, Ge, CdTe and HgI_2 single cylindrical detectors at 140.4 and 511 keV as functions of length and diameter. Error bars indicate upper and lower limits to the efficiency.

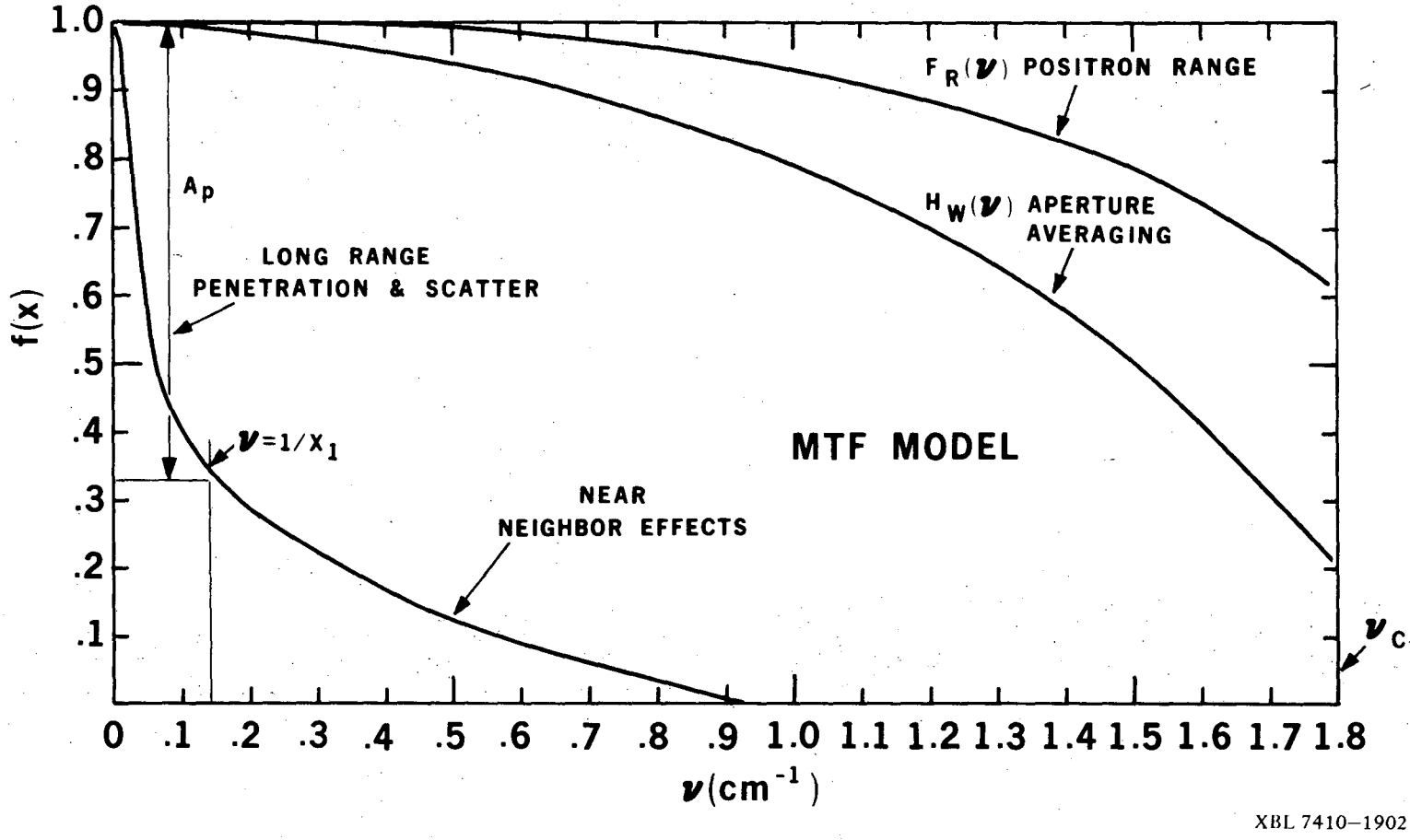
1.0
.9
.8
.7
.6
.5
.4
.3
.2
.1
f(x)
A_p
LONG RANGE
PENETRATION & SCATTER
$F_R(\nu)$ POSITRON RANGE
$H_W(\nu)$ APERTURE
AVERAGING
$\nu=1/X_1$
MTF MODEL
NEAR
NEIGHBOR EFFECTS
ν_c
0 .1 .2 .3 .4 .5 .6 .7 .8 .9 1.0 1.1 1.2 1.3 1.4 1.5 1.6 1.7 1.8
$\nu(cm^{-1})$
XBL 7410–1902

Fig. 1

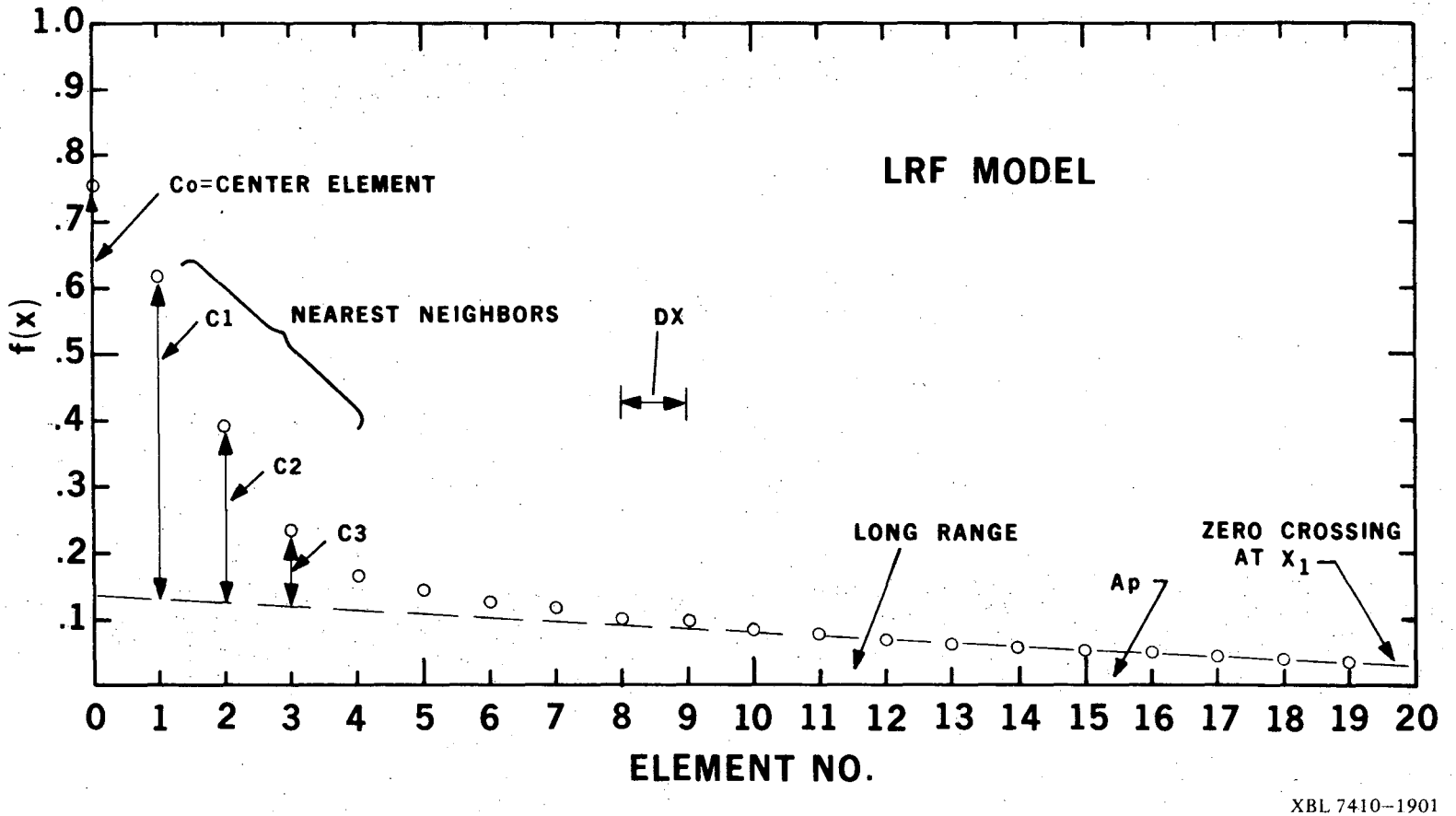

Fig. 2

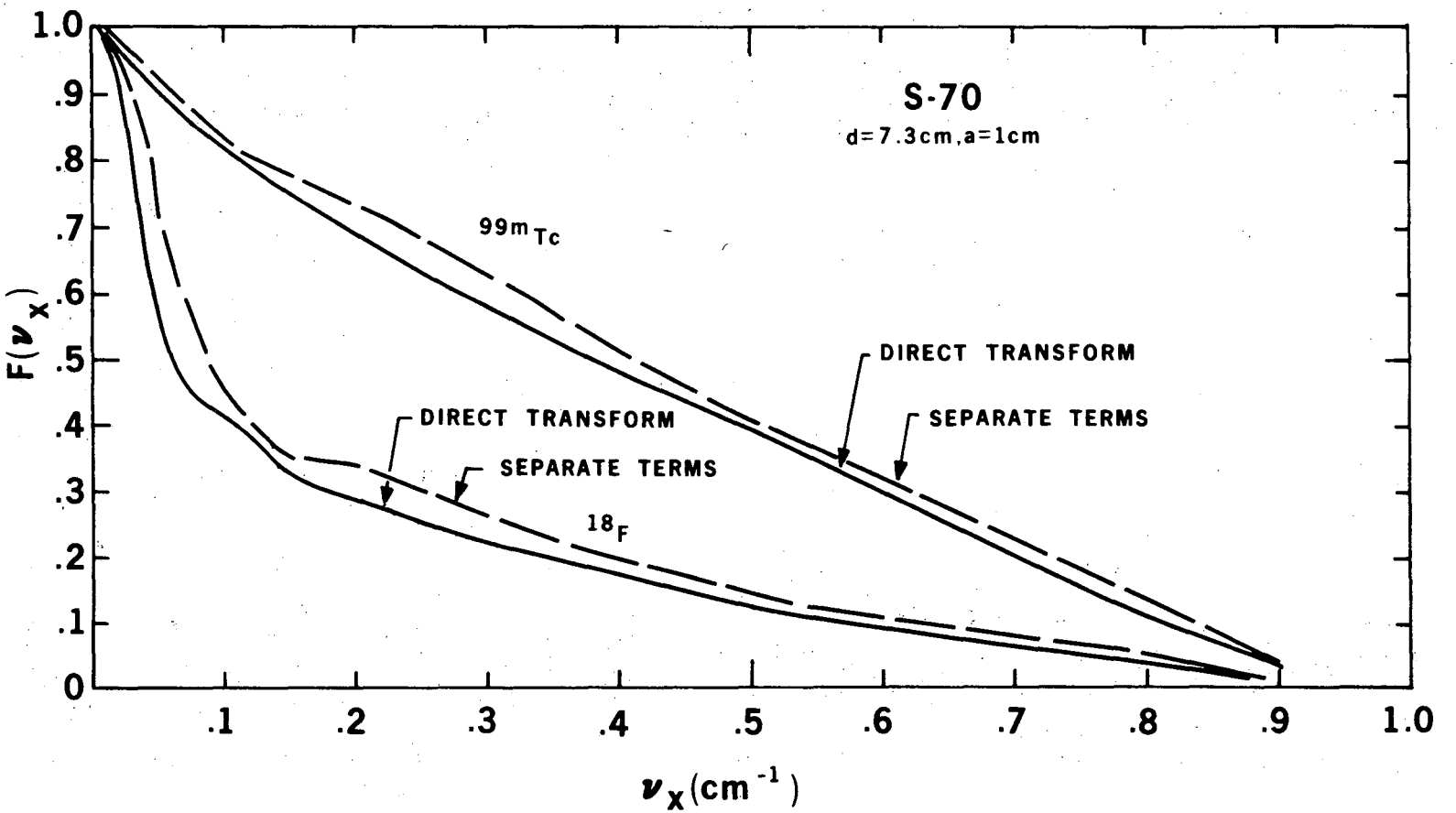

XBL 7410–1900

Fig. 3

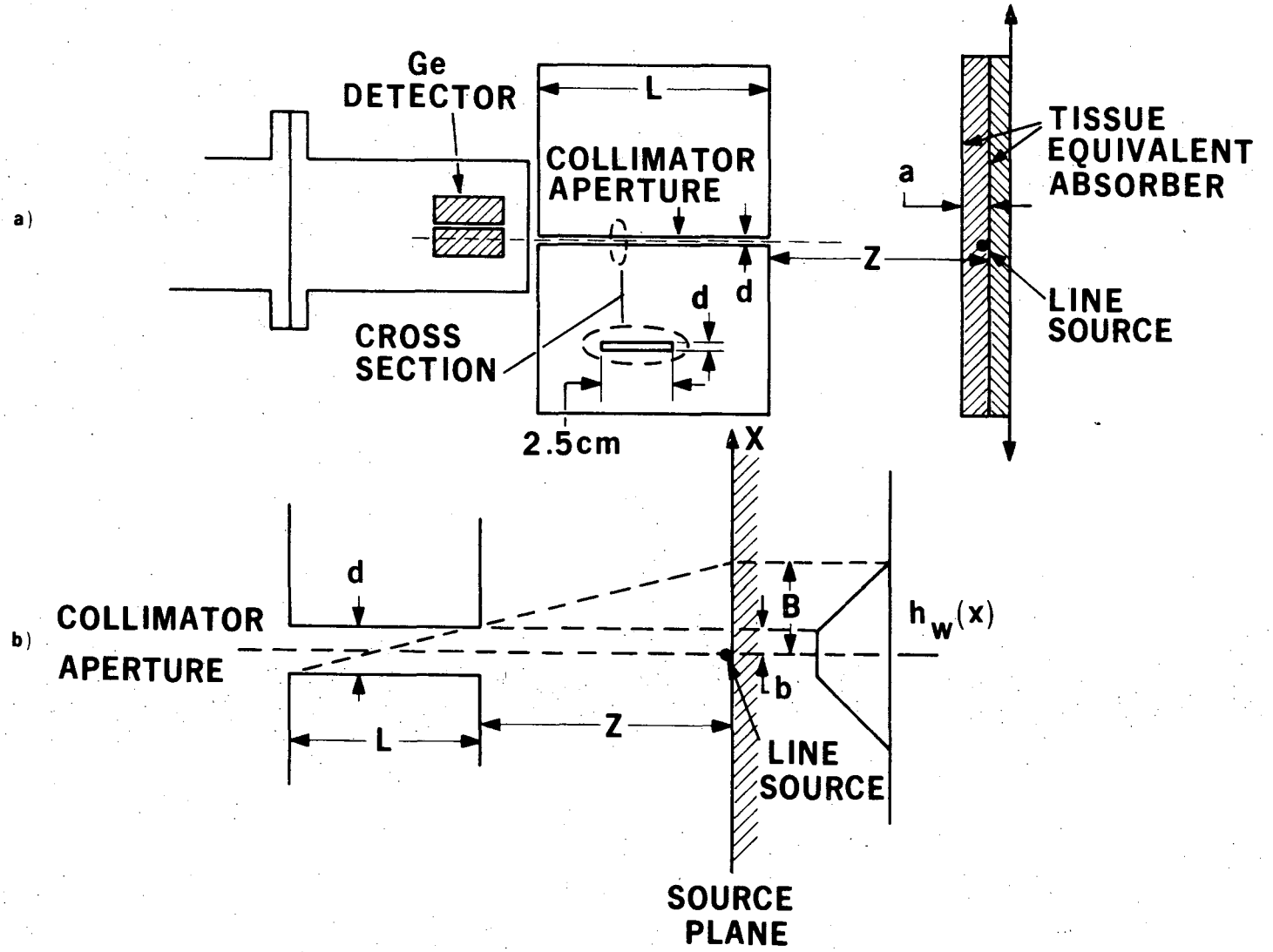

XBL 7410—1891

Fig. 4

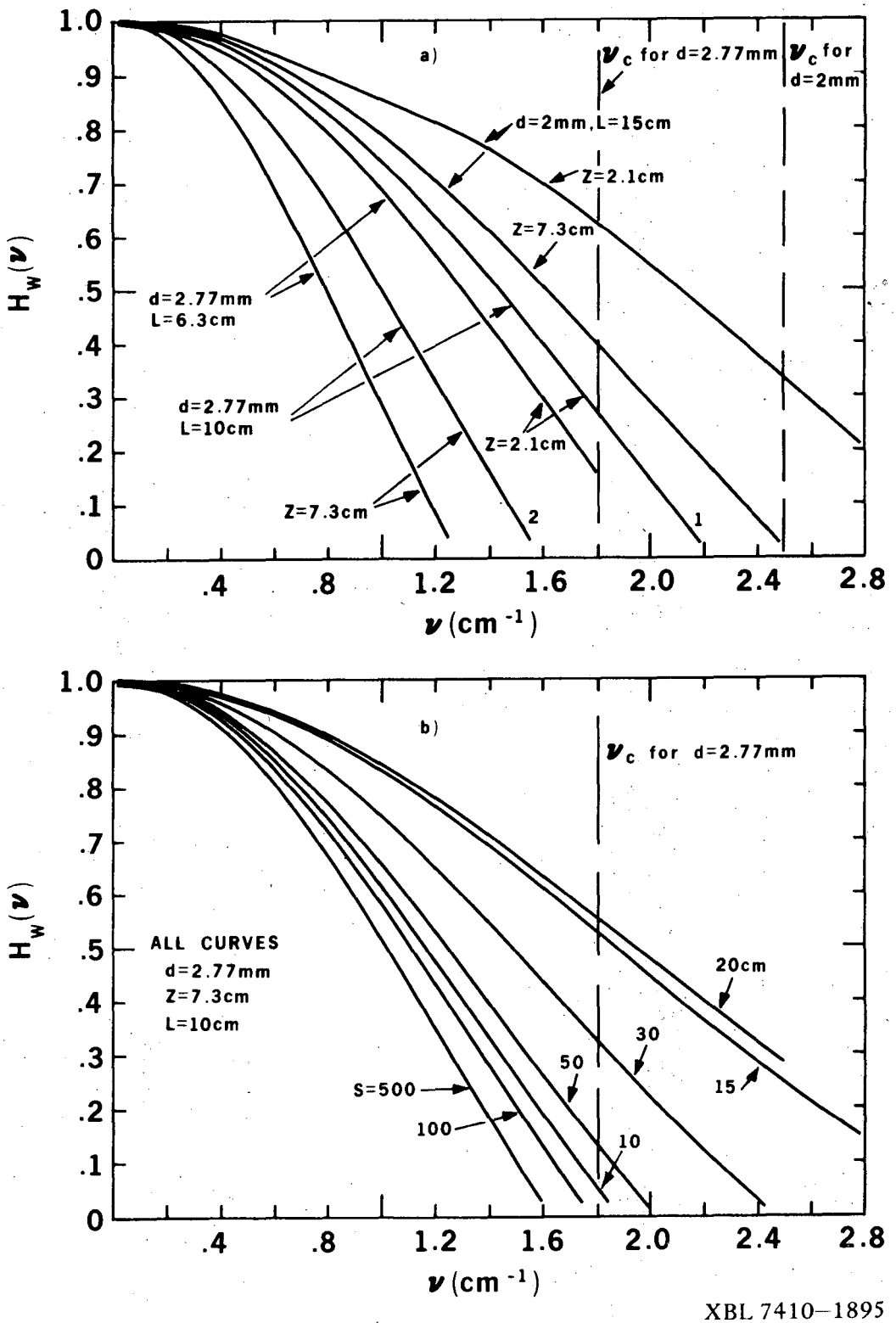
a)
ν_c for d=2.77mm
ν_c for d=2mm
d=2mm, L=15cm
Z=2.1cm
Z=7.3cm
d=2.77mm L=6.3cm
d=2.77mm L=10cm
Z=2.1cm
Z=7.3cm
2
1
$H_w(\nu)$
ν (cm^{-1})
b)
ν_c for d=2.77mm
ALL CURVES
d=2.77mm
Z=7.3cm
L=10cm
20cm
30
50
15
S=500
100
10
$H_w(\nu)$
ν (cm^{-1})
XBL 7410—1895

Fig. 5

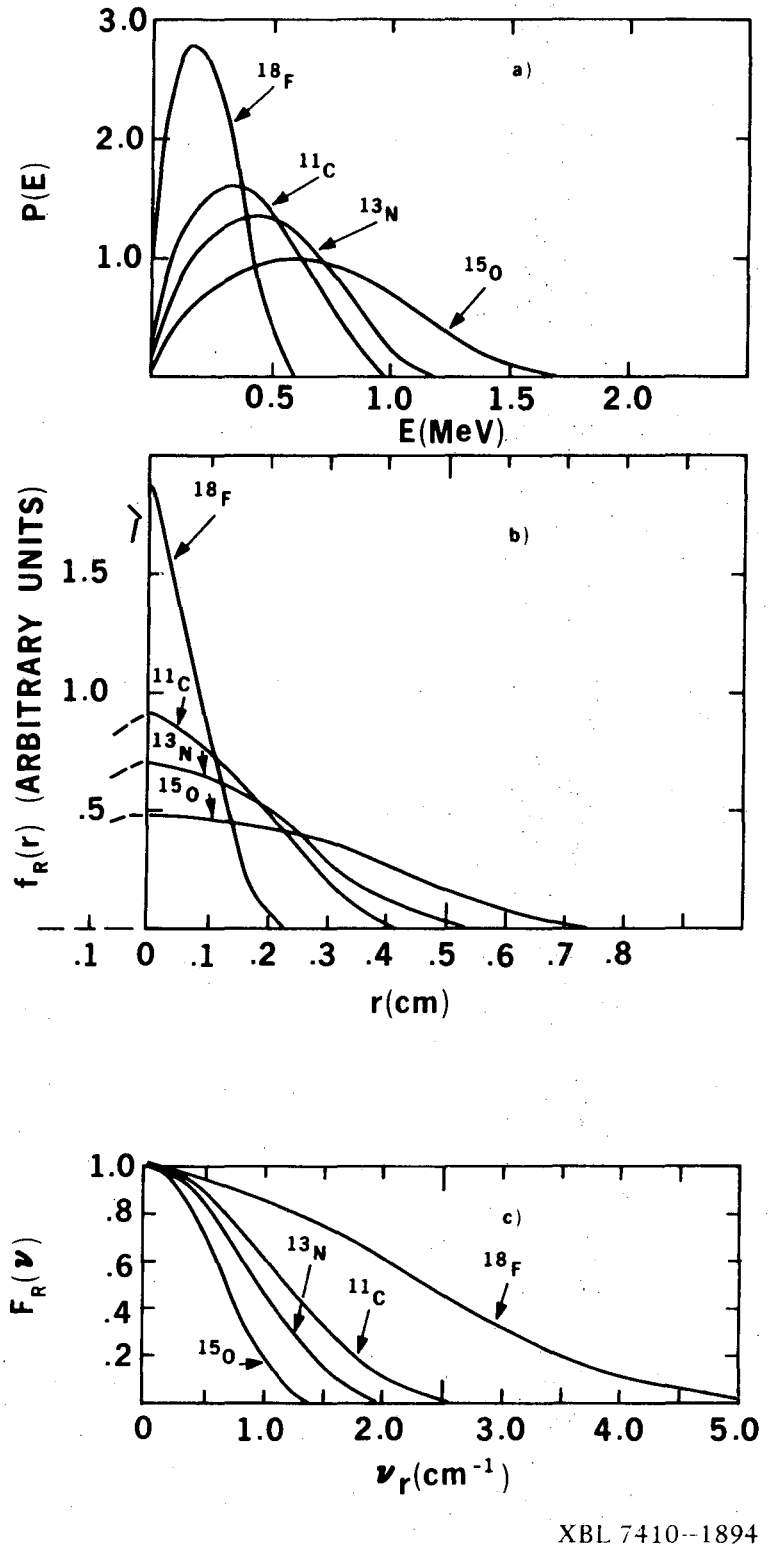

XBL 7410--1894

Fig. 6

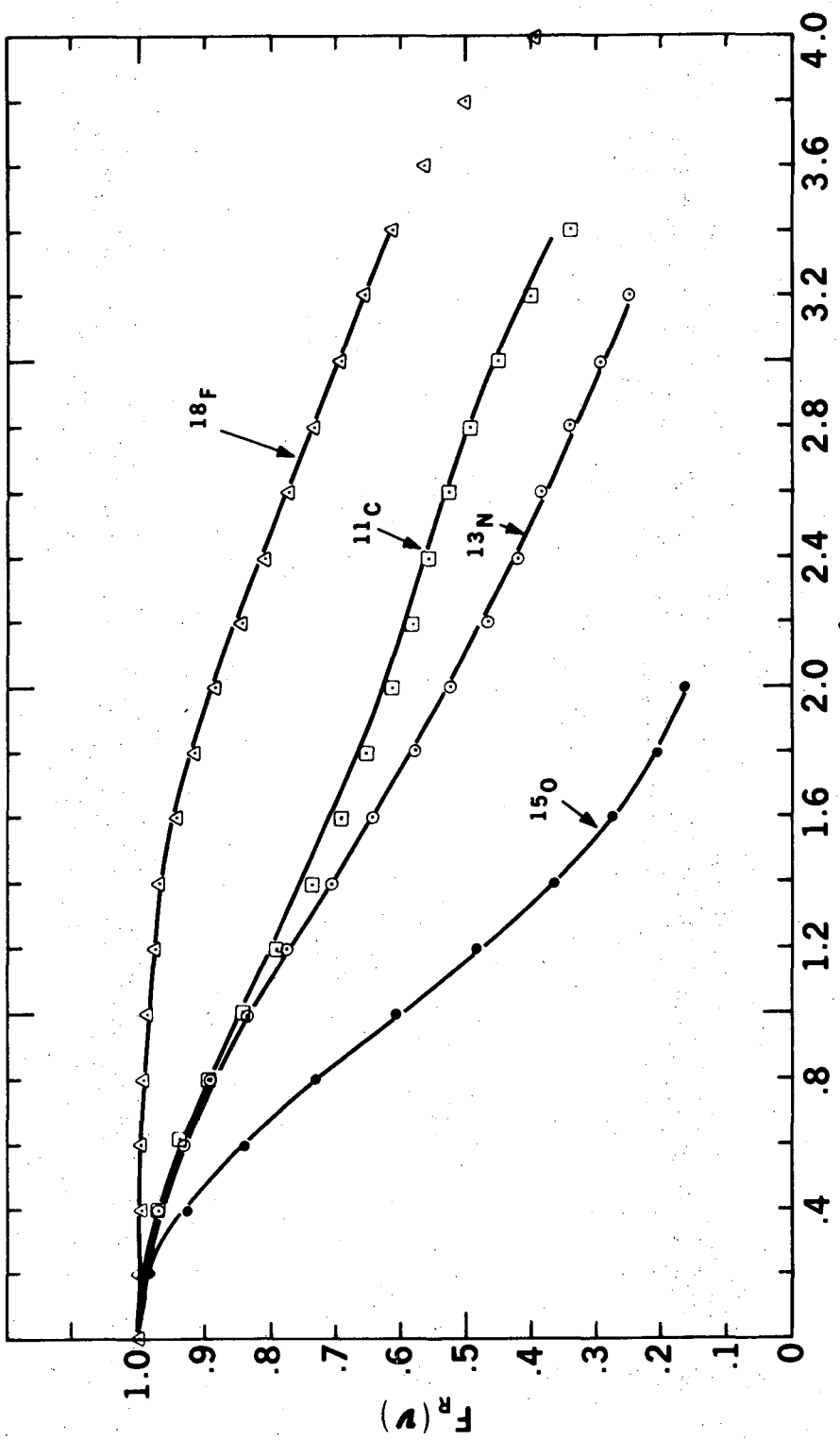

XBL 7410-1896

Fig. 7

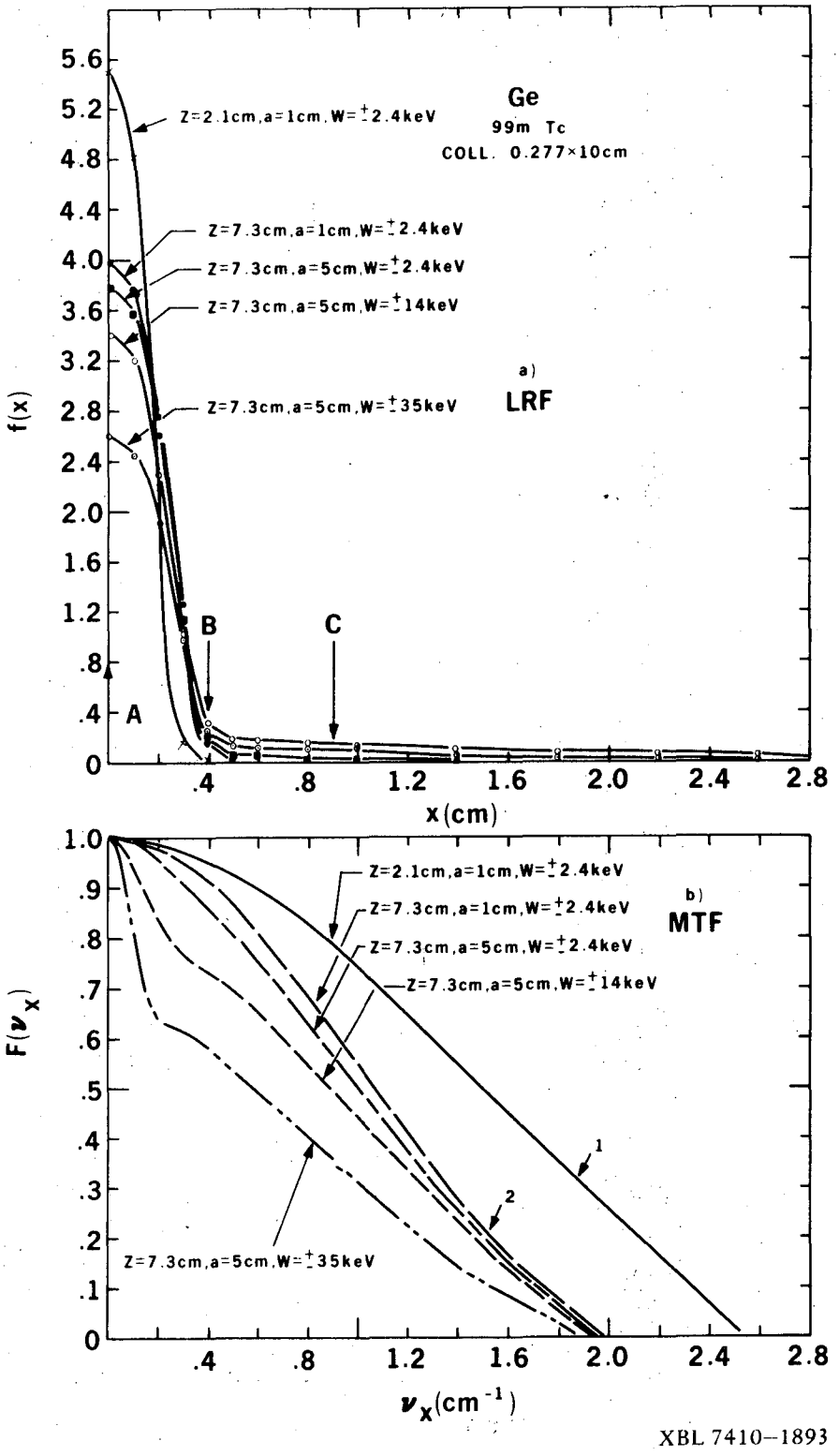

Fig. 8

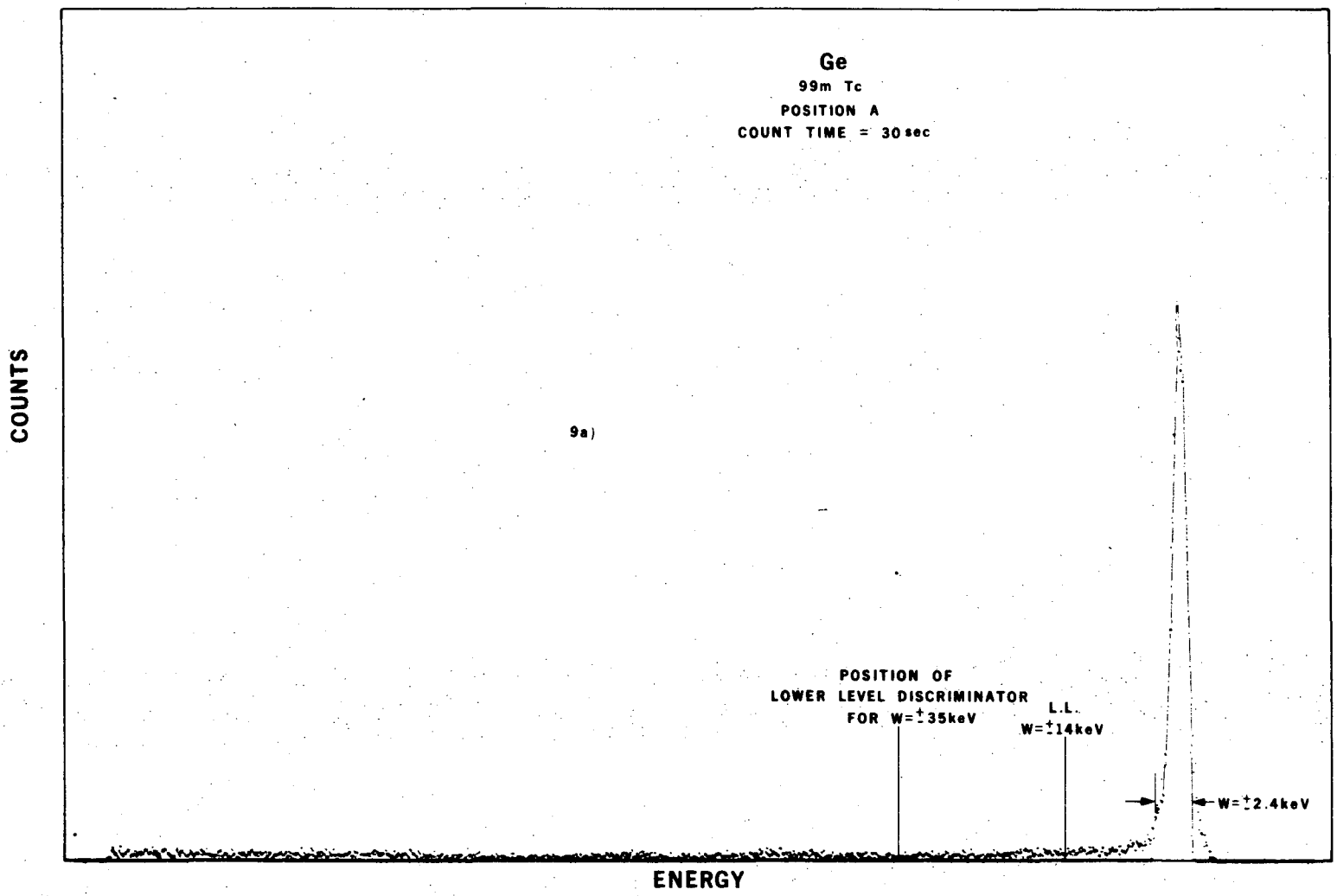
Ge
99m Tc
POSITION A
COUNT TIME = 30 sec
9a)
COUNTS
POSITION OF
LOWER LEVEL DISCRIMINATOR
FOR W=±35keV
L.L.
W=±14keV
W=±2.4keV
ENERGY
XBL 7410-1888

Fig. 9a

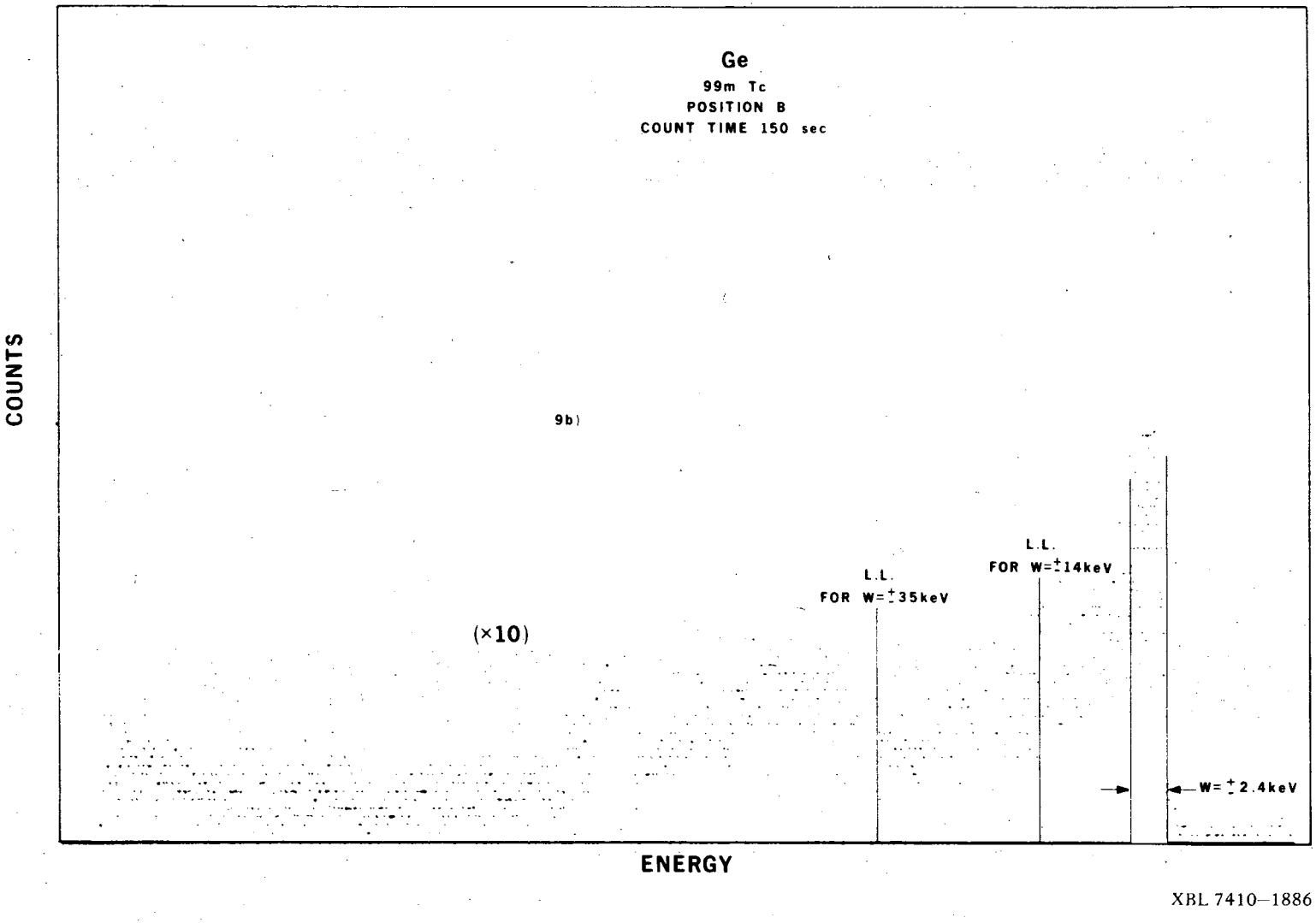

XBL 7410–1886

Fig. 9b

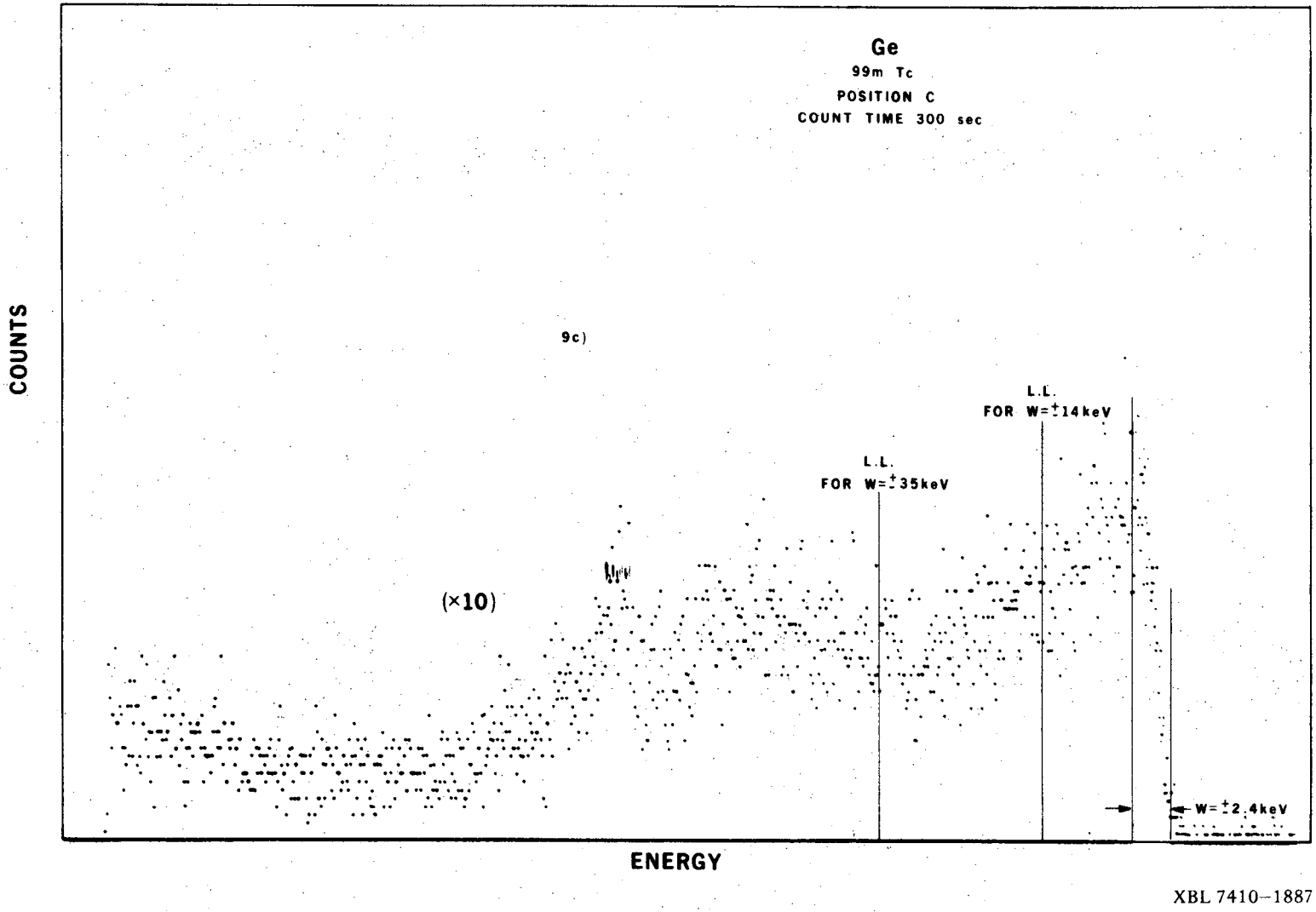

XBL 7410-1887

Fig. 9c

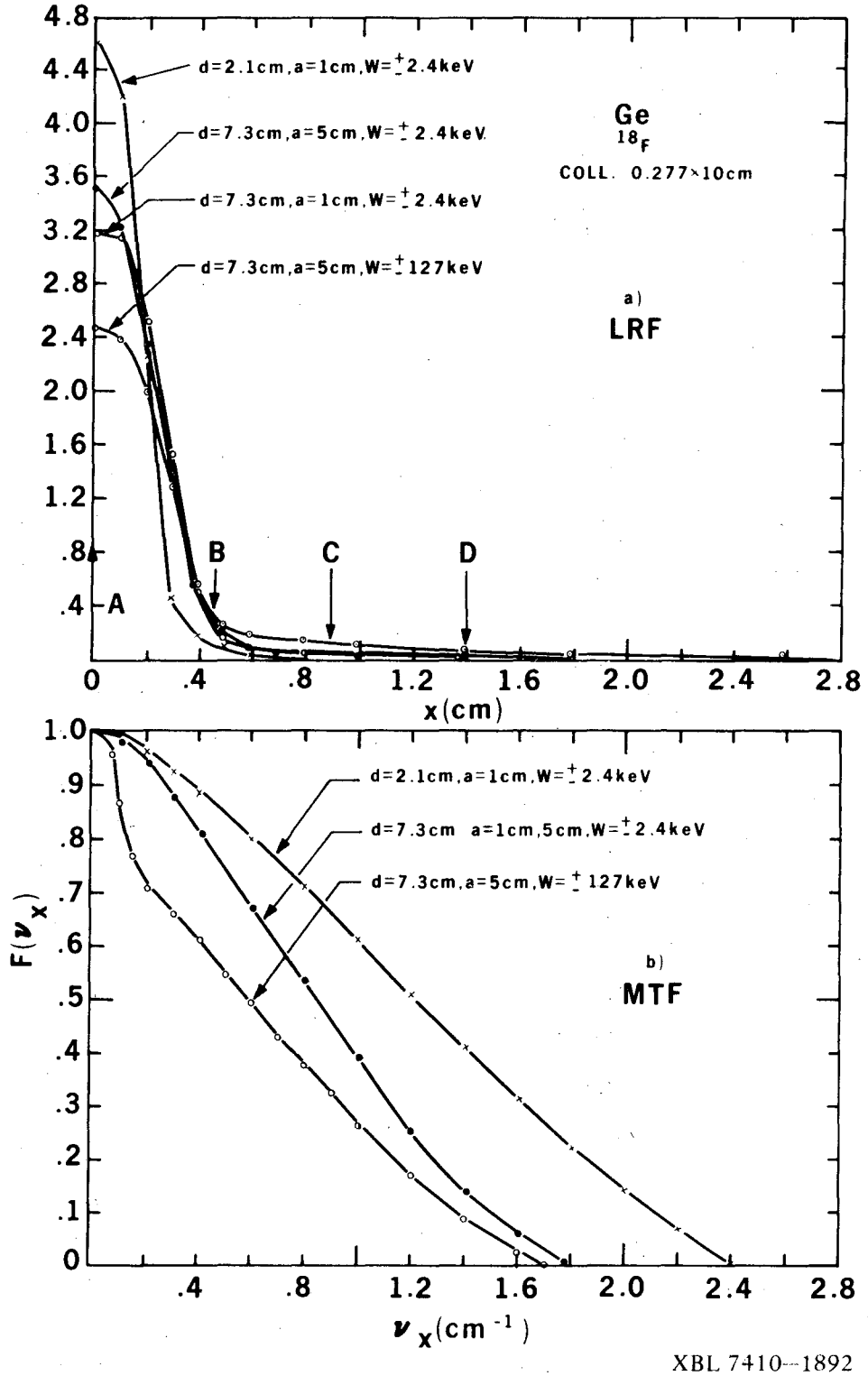

XBL 7410--1892

Fig. 10

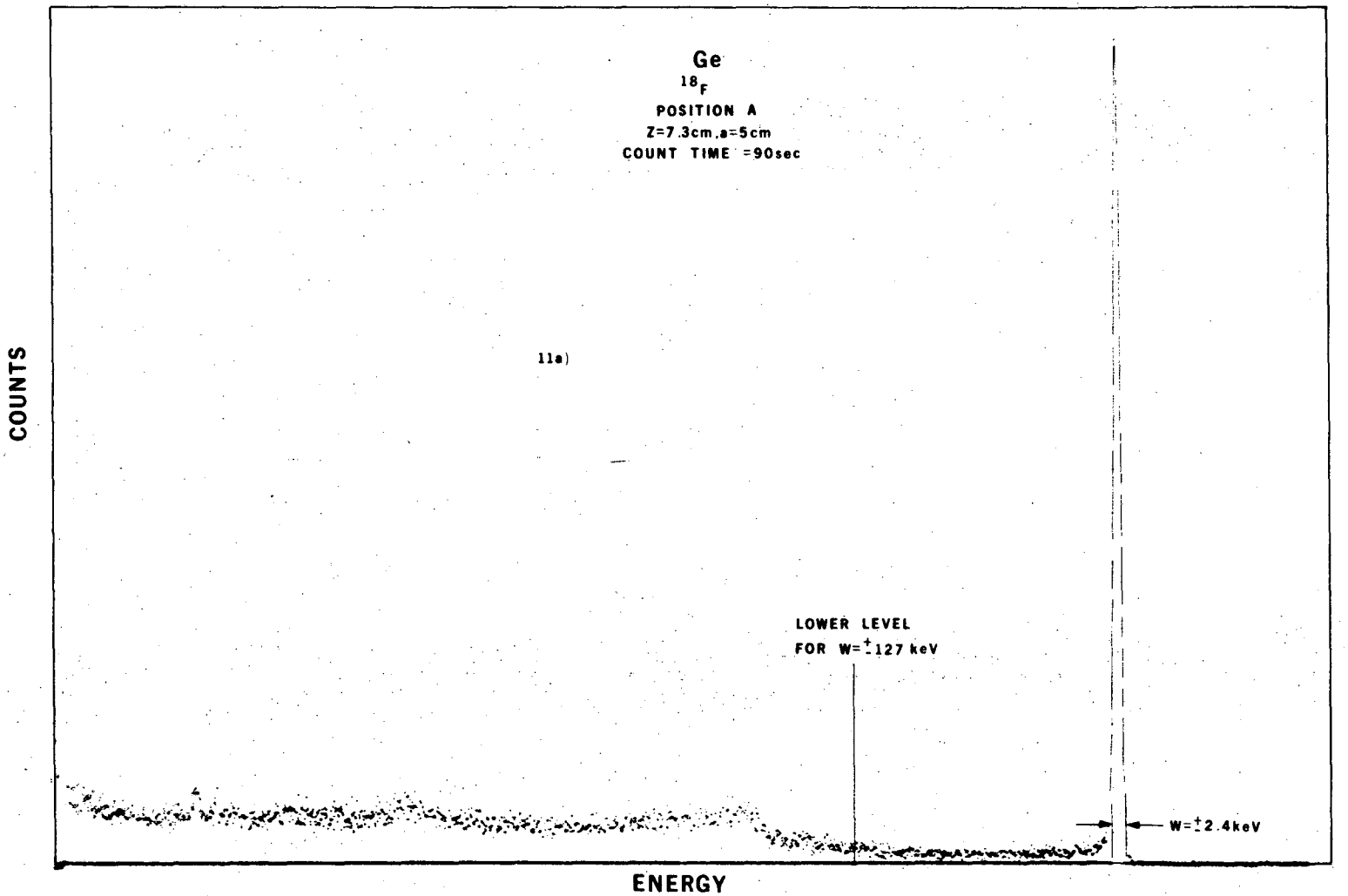

XBL 7410–1884

Fig. 11a

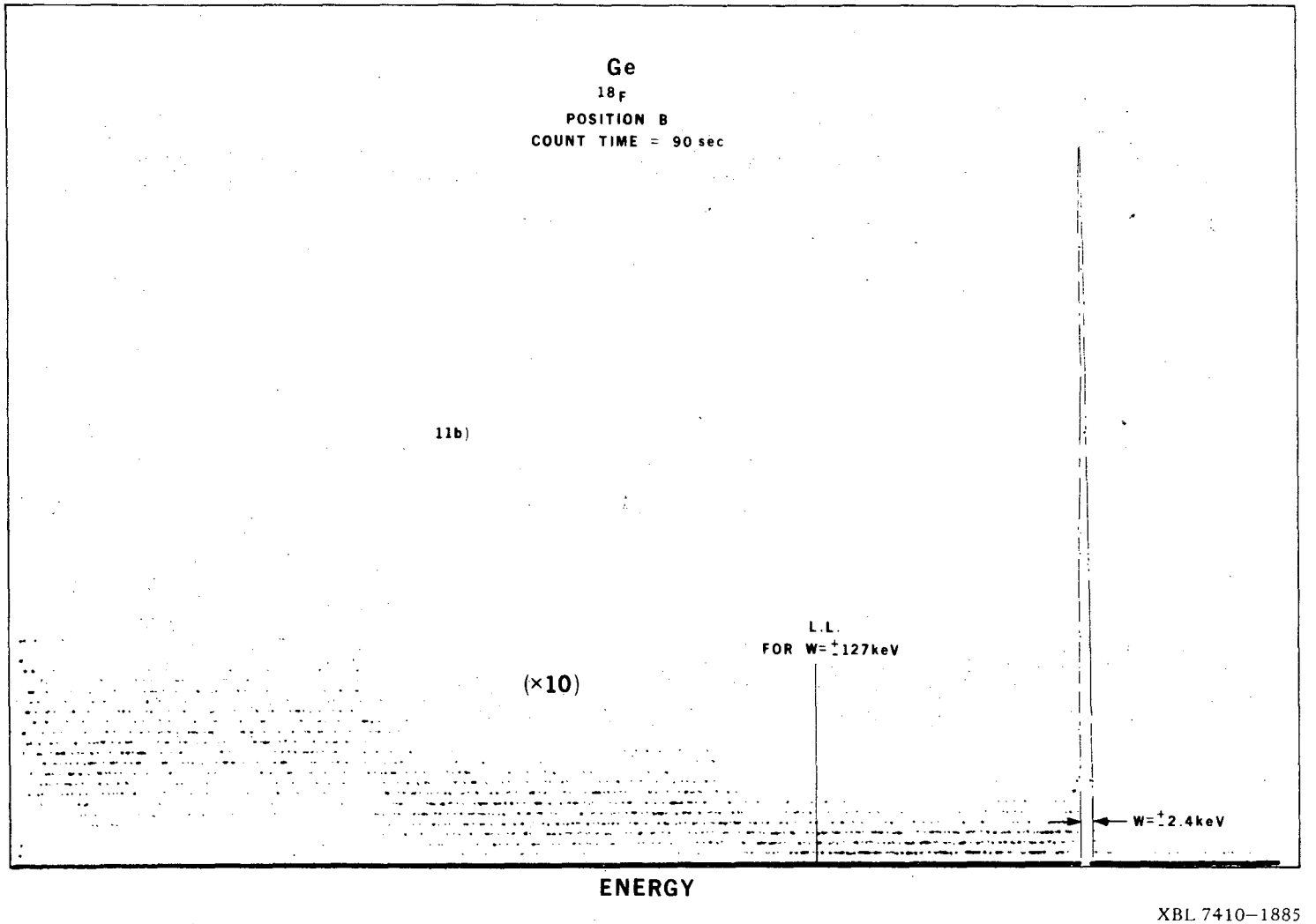

XBL 7410–1885

Fig. 11b

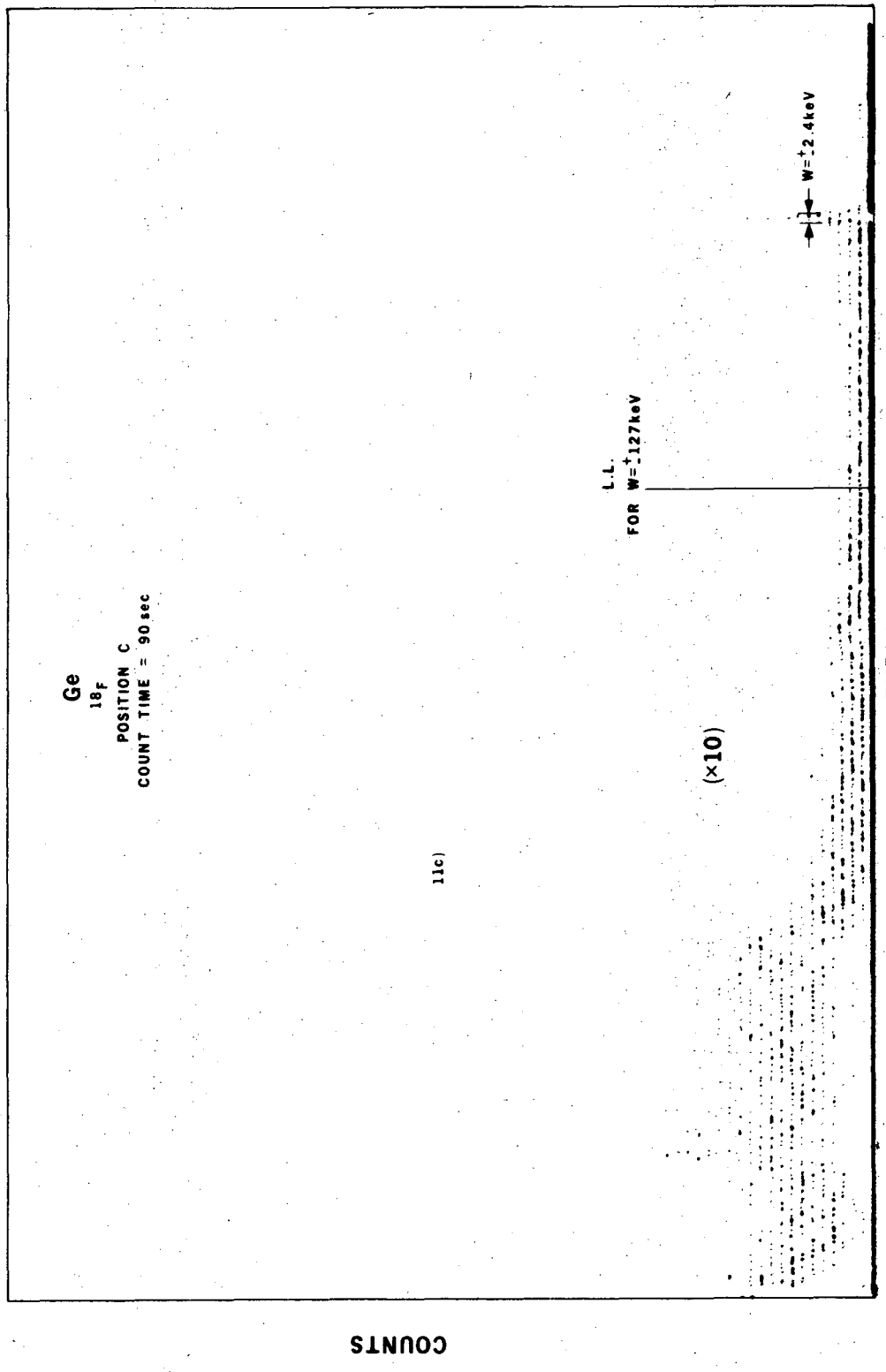

XBL 7410-1889

Fig. 11c

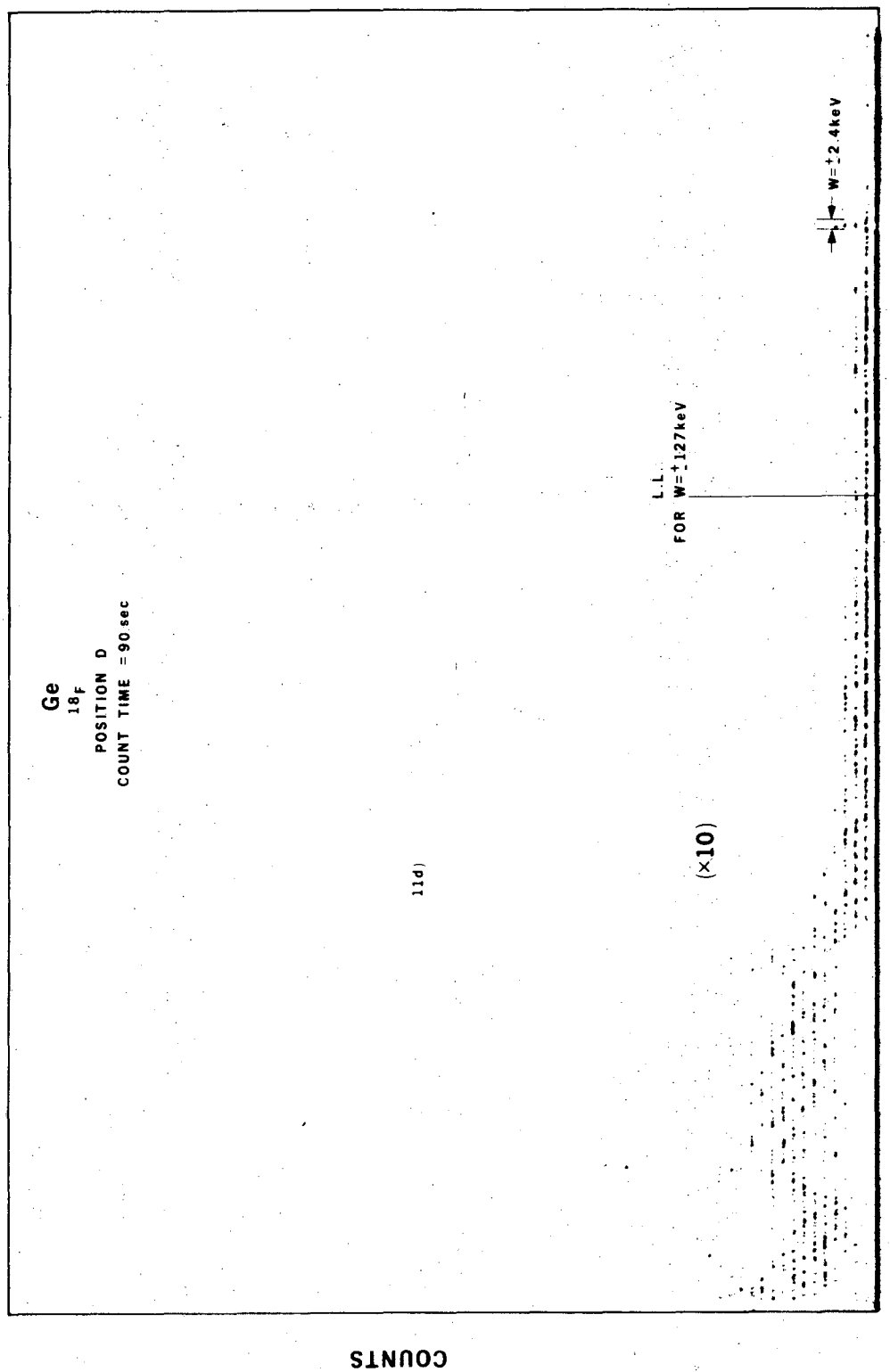

XBL 7410-1890

Fig. 11d

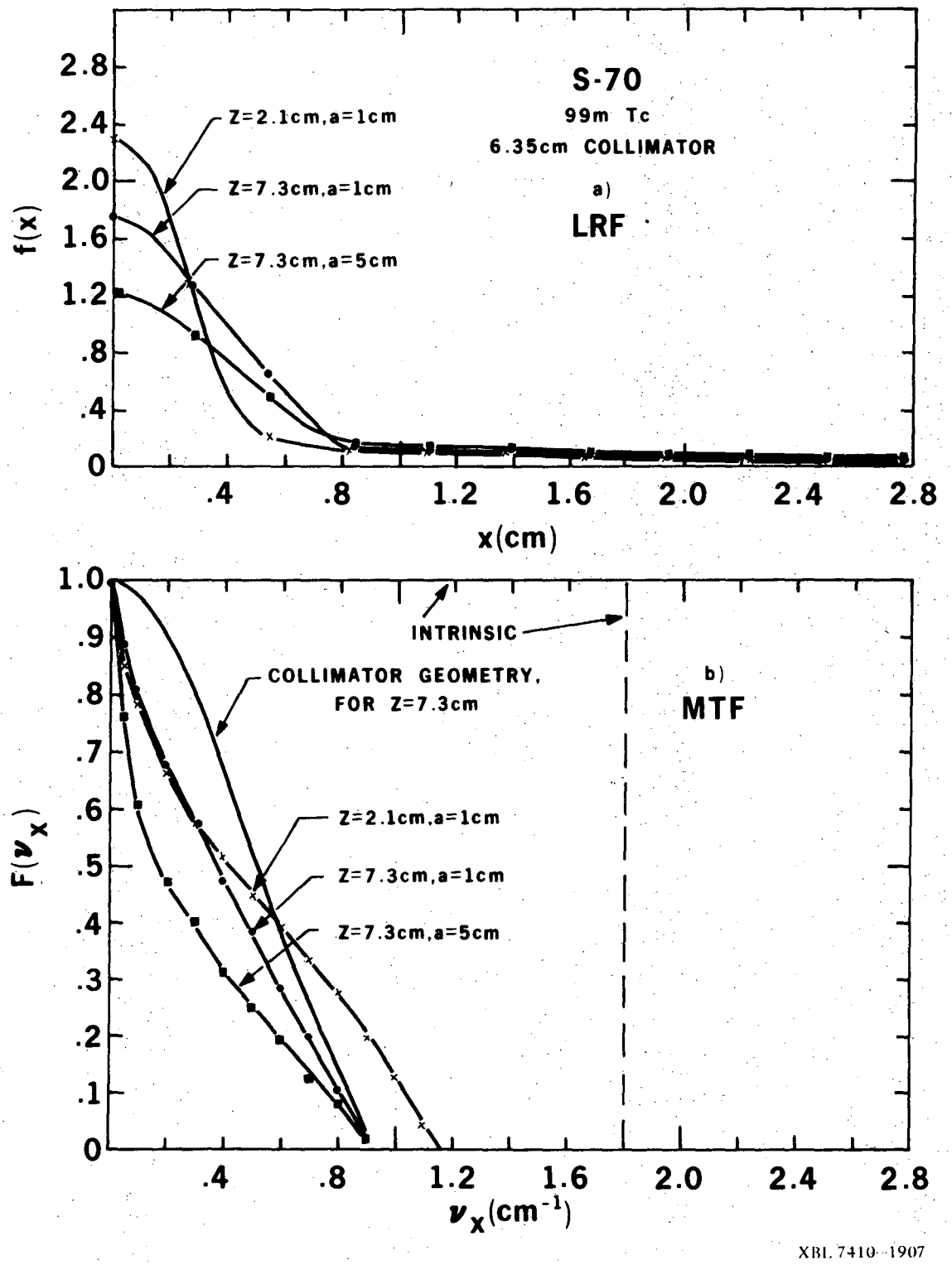
S-70
99m Tc
6.35cm COLLIMATOR
a)
LRF
Z=2.1cm,a=1cm
Z=7.3cm,a=1cm
Z=7.3cm,a=5cm
f(x)
x(cm)
INTRINSIC
COLLIMATOR GEOMETRY,
FOR Z=7.3cm
b)
MTF
Z=2.1cm,a=1cm
Z=7.3cm,a=1cm
Z=7.3cm,a=5cm
F(ν_x)
ν_x(cm^-1)
XBL 7410-1907

Fig. 12

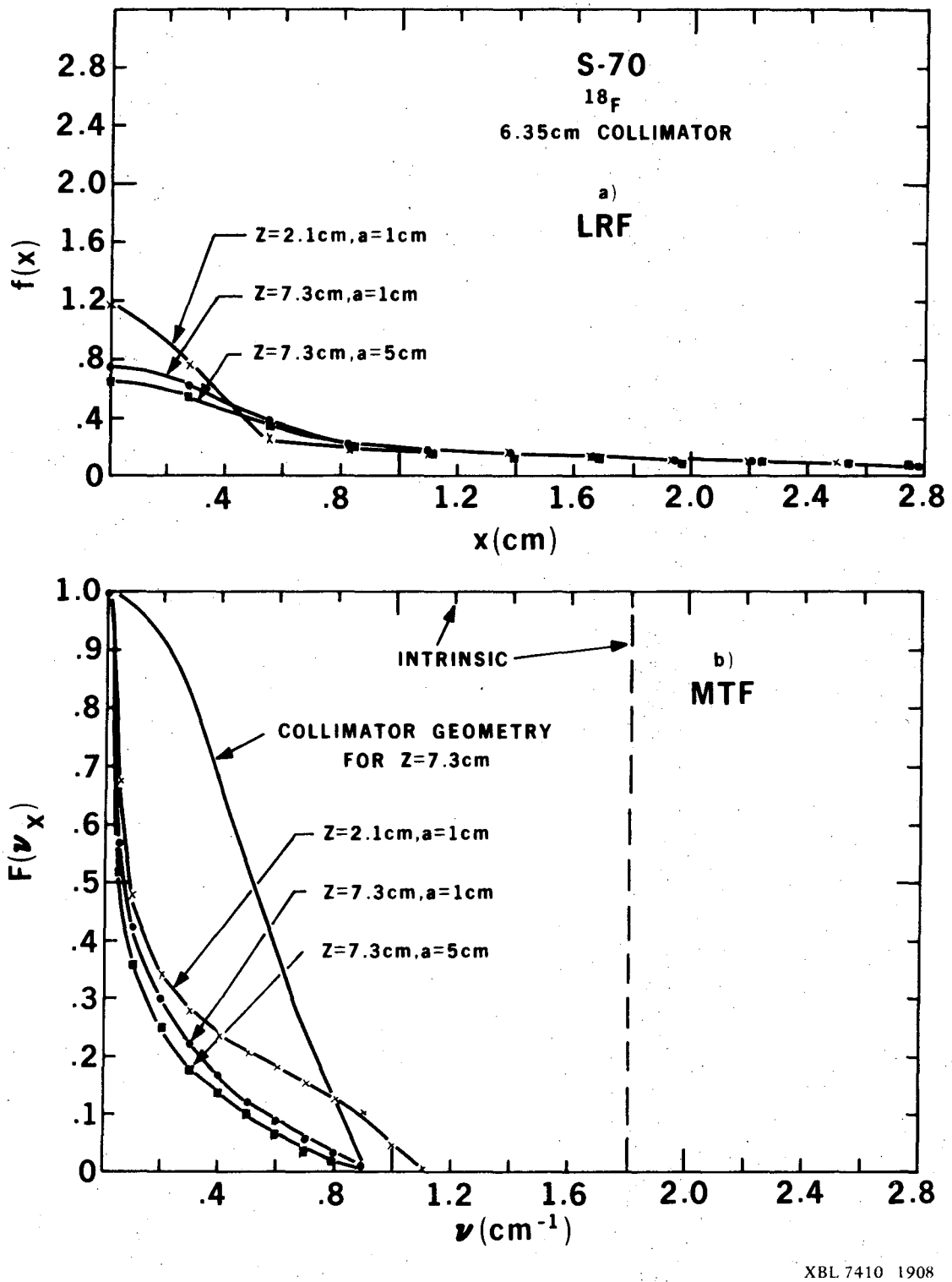

Fig. 13

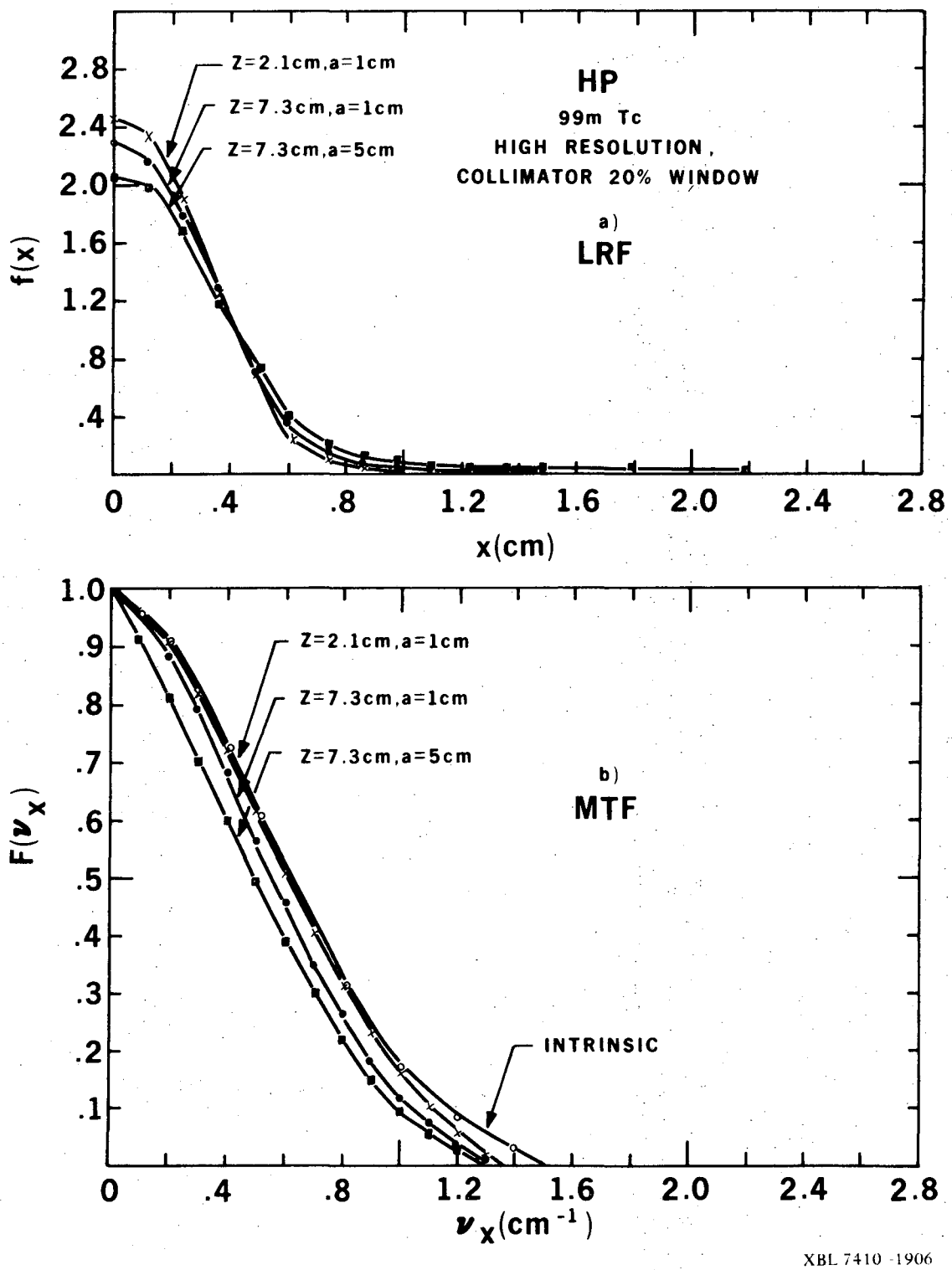
HP
99m Tc
HIGH RESOLUTION,
COLLIMATOR 20% WINDOW
a)
LRF
Z=2.1cm,a=1cm
Z=7.3cm,a=1cm
Z=7.3cm,a=5cm
f(x)
x(cm)
b)
MTF
INTRINSIC
F(ν_x)
ν_x(cm^-1)
XBL 7410 -1906

Fig. 14

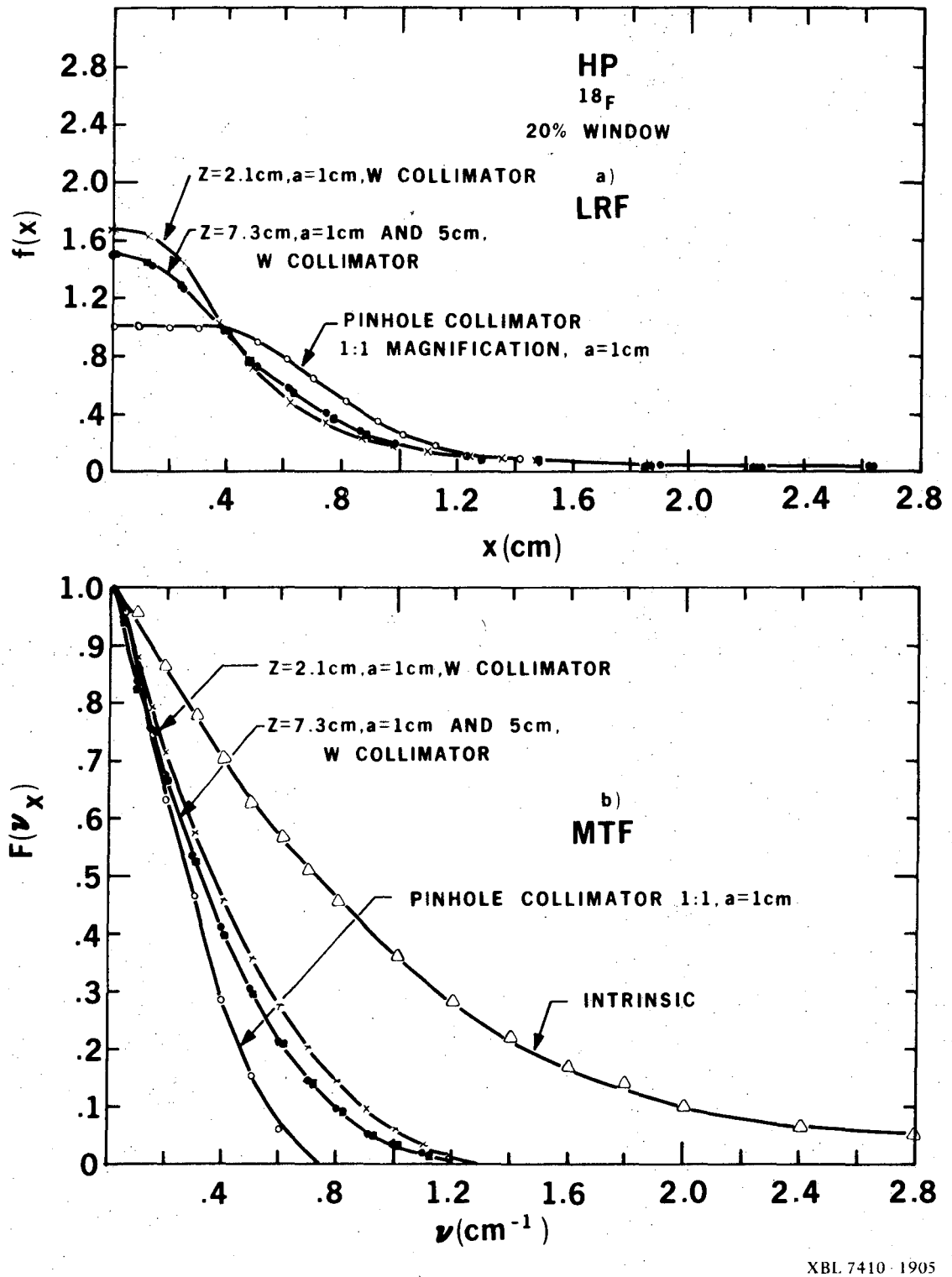

Fig. 15

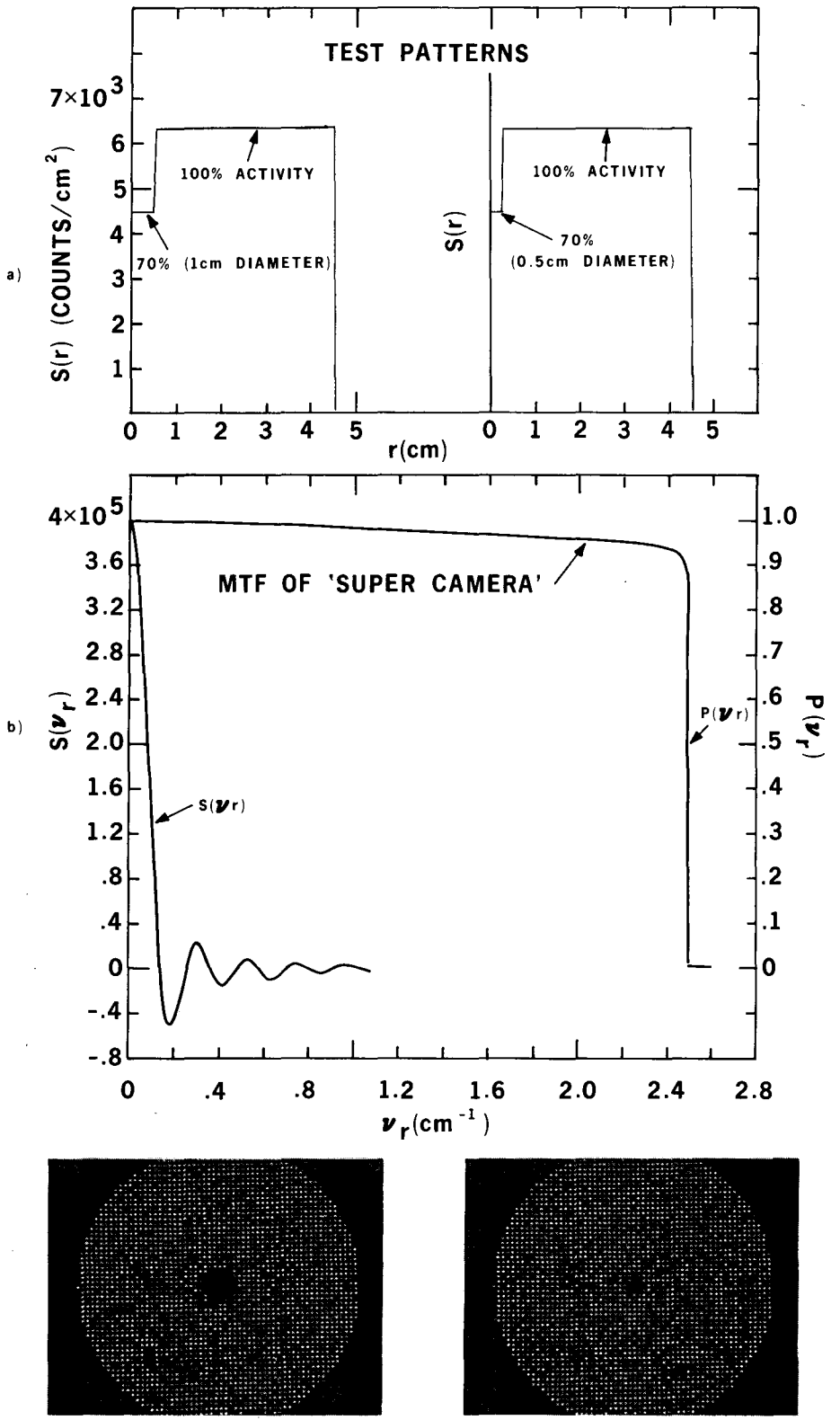

XBB 7410-7019

Fig. 16

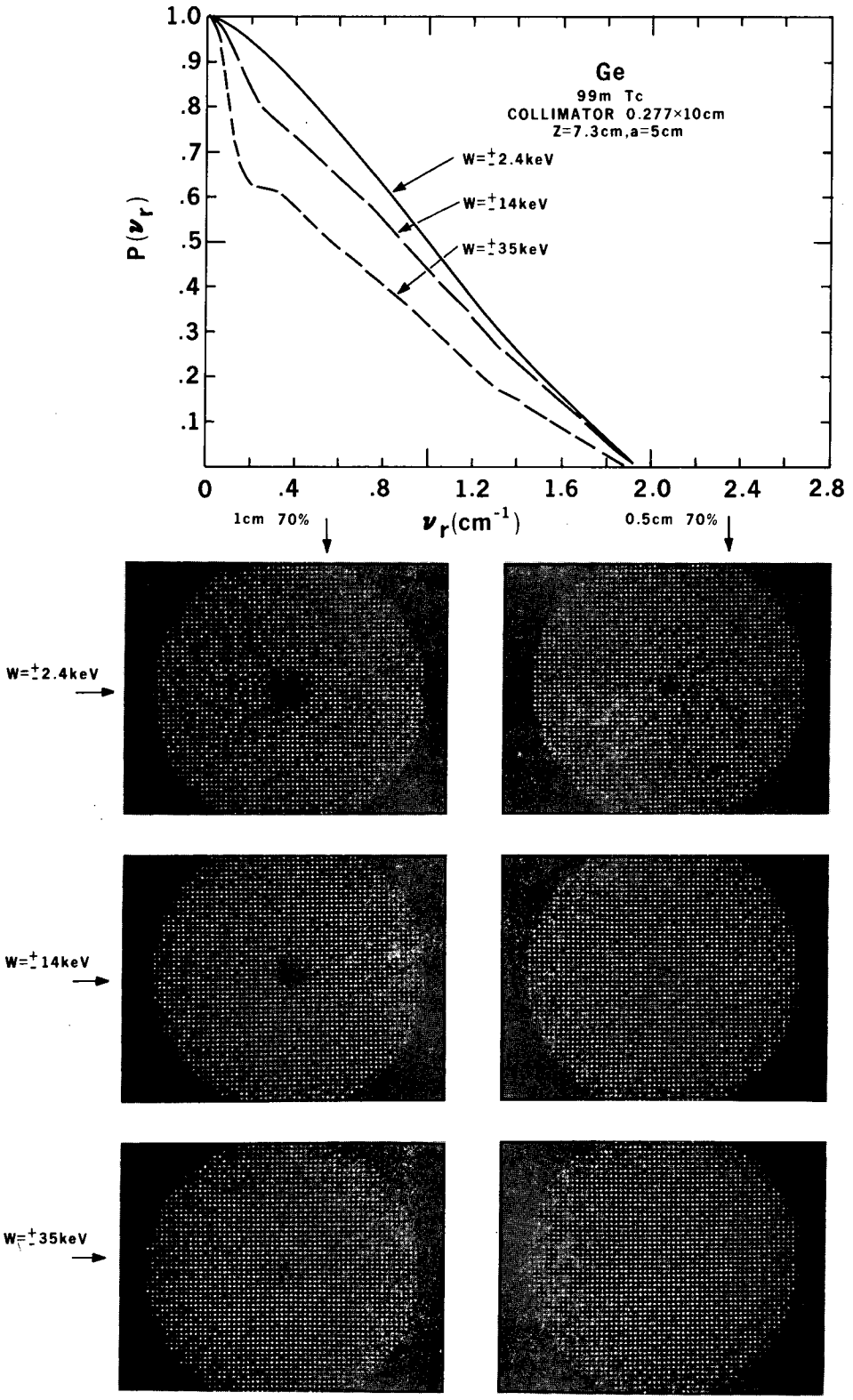

XBB 7410-7020

Fig. 17

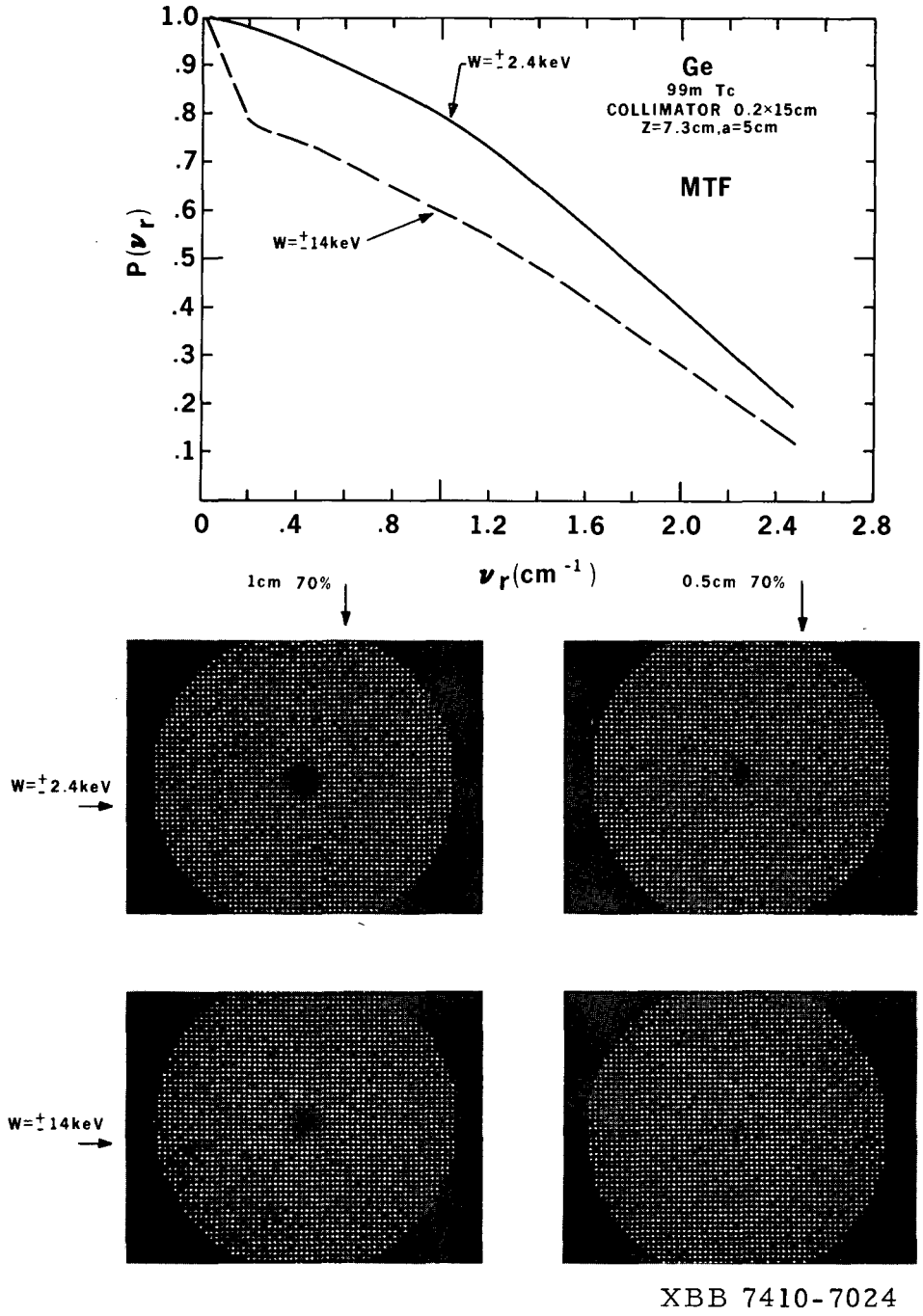
1.0
.9
.8
.7
.6
.5
.4
.3
.2
.1
P(ν_r)
W=±2.4keV
W=±14keV
Ge
99m Tc
COLLIMATOR 0.2×15cm
Z=7.3cm,a=5cm
MTF
0
.4
.8
1.2
1.6
2.0
2.4
2.8
ν_r(cm^-1)
1cm 70%
0.5cm 70%
W=±2.4keV
W=±14keV
XBB 7410-7024

Fig. 18

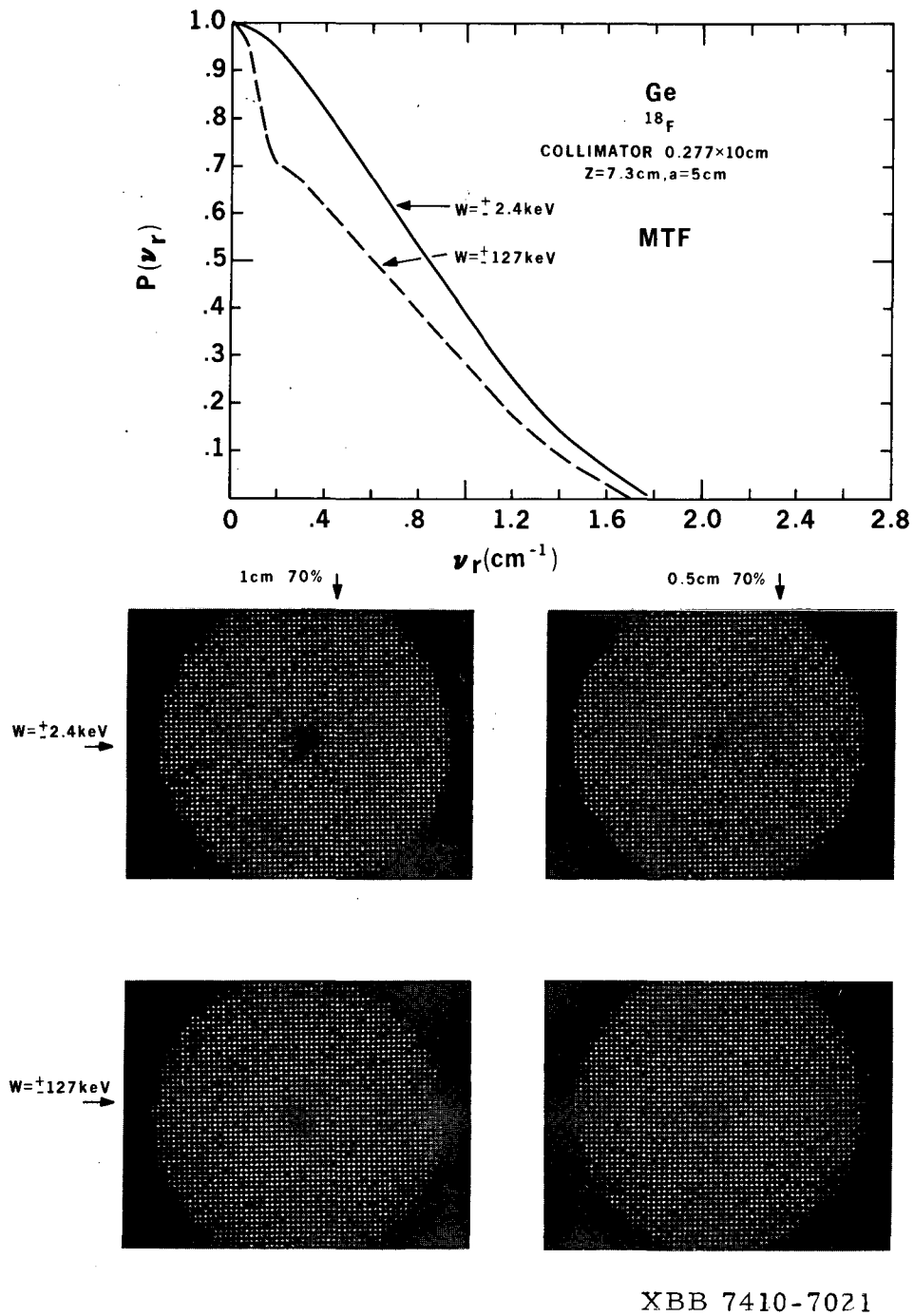

Fig. 19

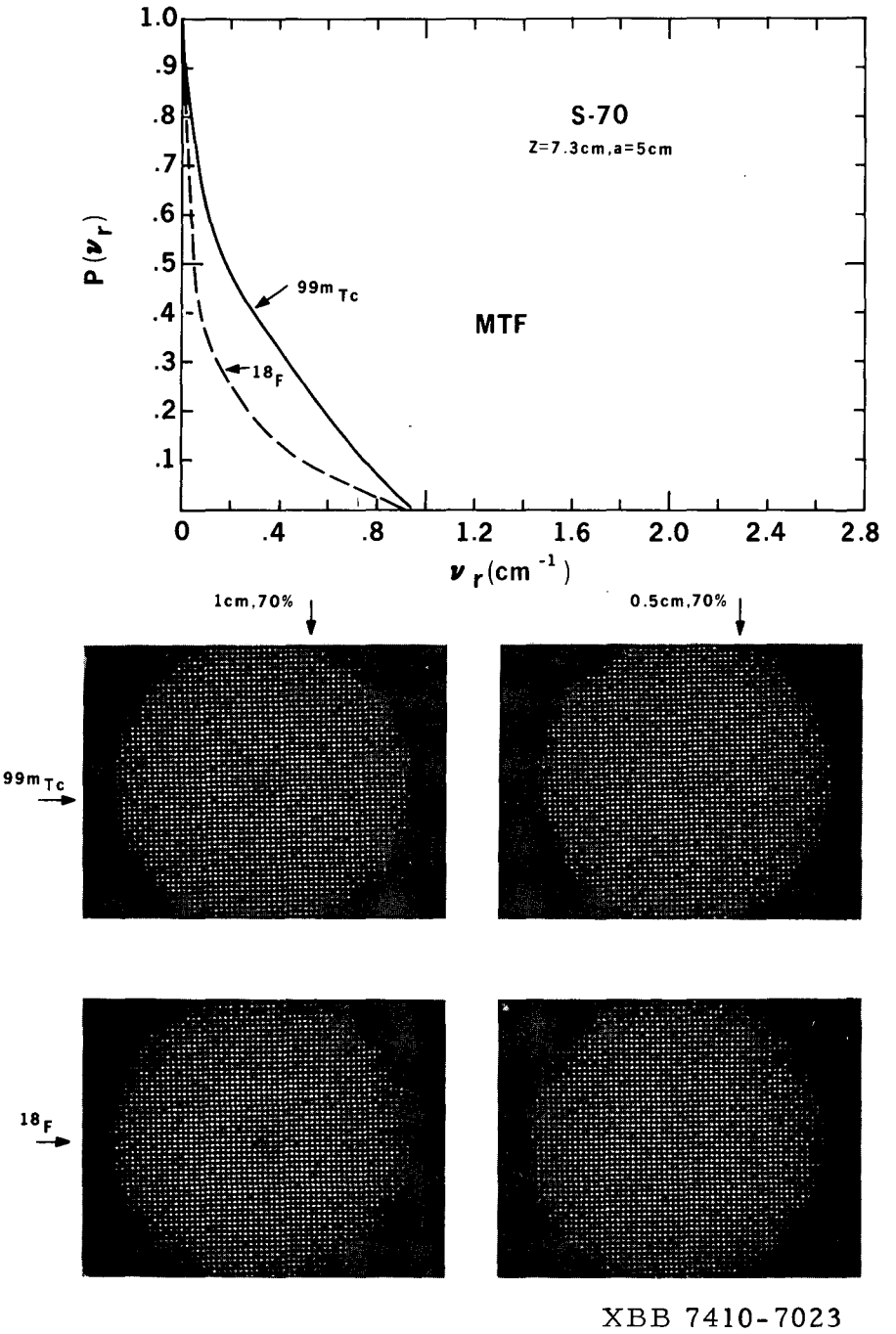
1.0
.9
.8
.7
.6
.5
.4
.3
.2
.1
P(ν_r)
S-70
Z=7.3cm,a=5cm
99m Tc
MTF
18 F
0
.4
.8
1.2
1.6
2.0
2.4
2.8
ν_r(cm^-1)
1cm,70%
0.5cm,70%
99m Tc
18 F
XBB 7410-7023

Fig. 20

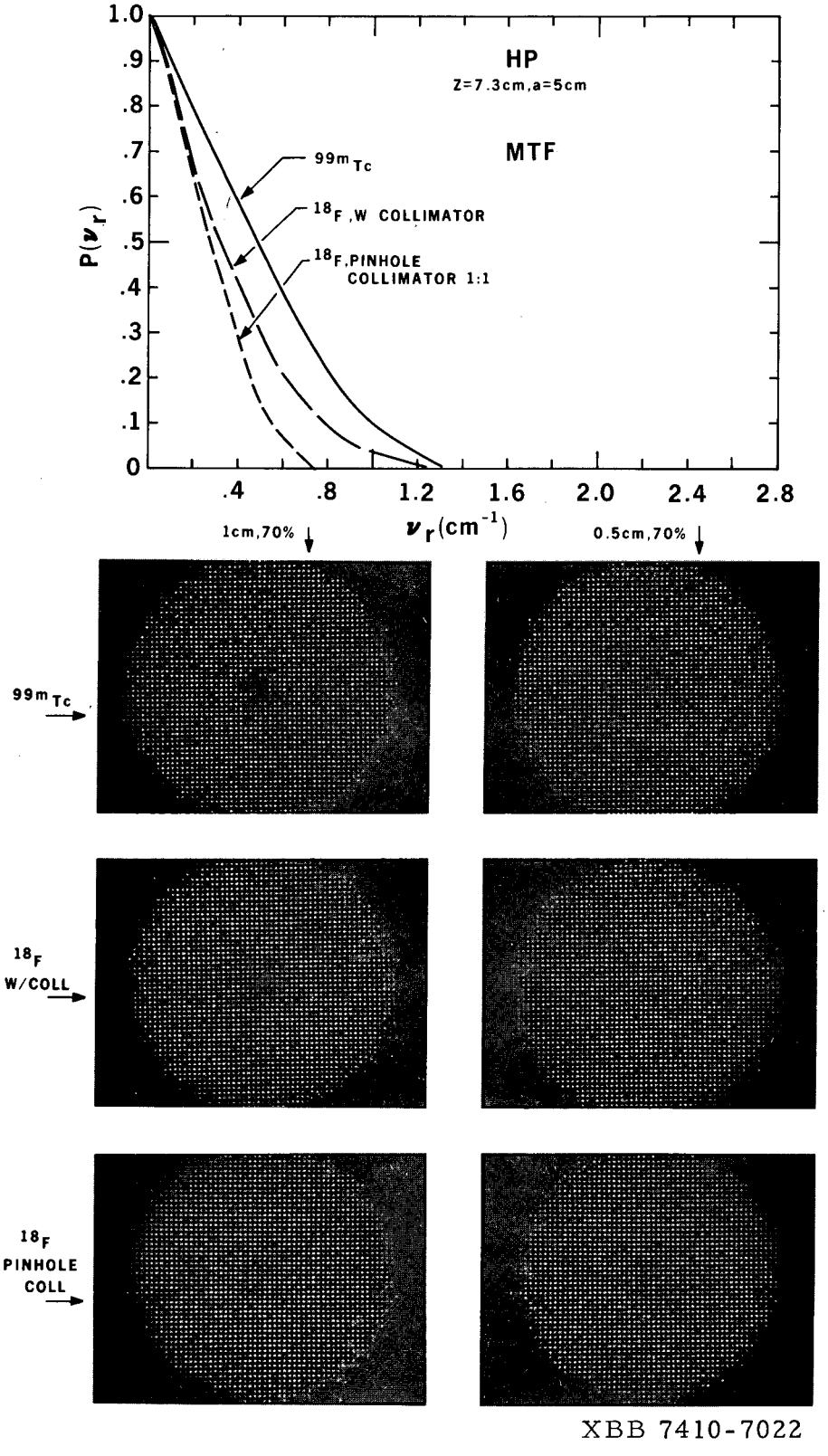

Fig. 21

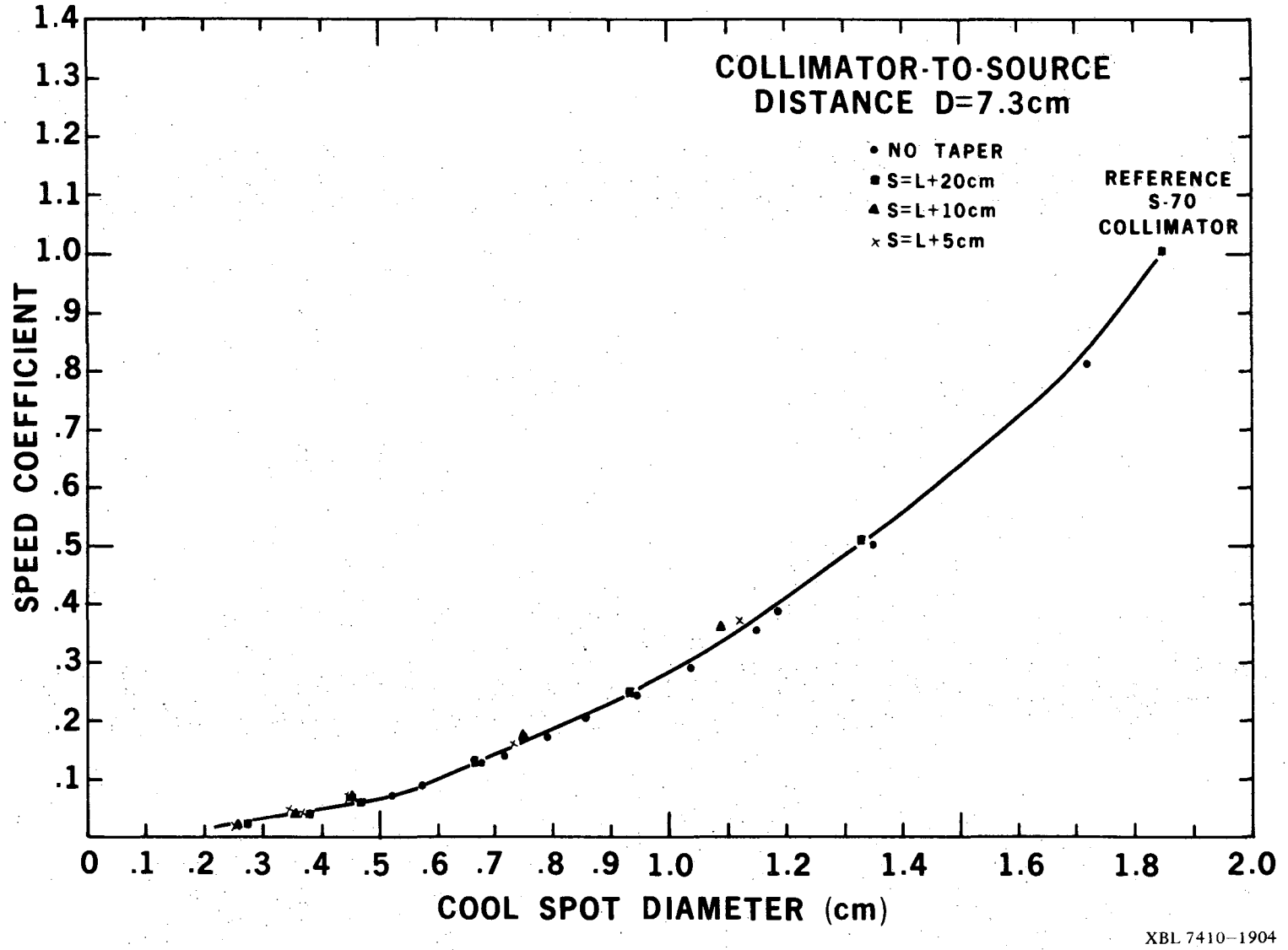
COLLIMATOR-TO-SOURCE
DISTANCE D=7.3cm
• NO TAPER
■ S=L+20cm
▲ S=L+10cm
× S=L+5cm
REFERENCE
S-70
COLLIMATOR
SPEED COEFFICIENT
1.4
1.3
1.2
1.1
1.0
.9
.8
.7
.6
.5
.4
.3
.2
.1
0 .1 .2 .3 .4 .5 .6 .7 .8 .9 1.0 1.2 1.4 1.6 1.8 2.0
COOL SPOT DIAMETER (cm)
XBL 7410-1904

Fig. 22

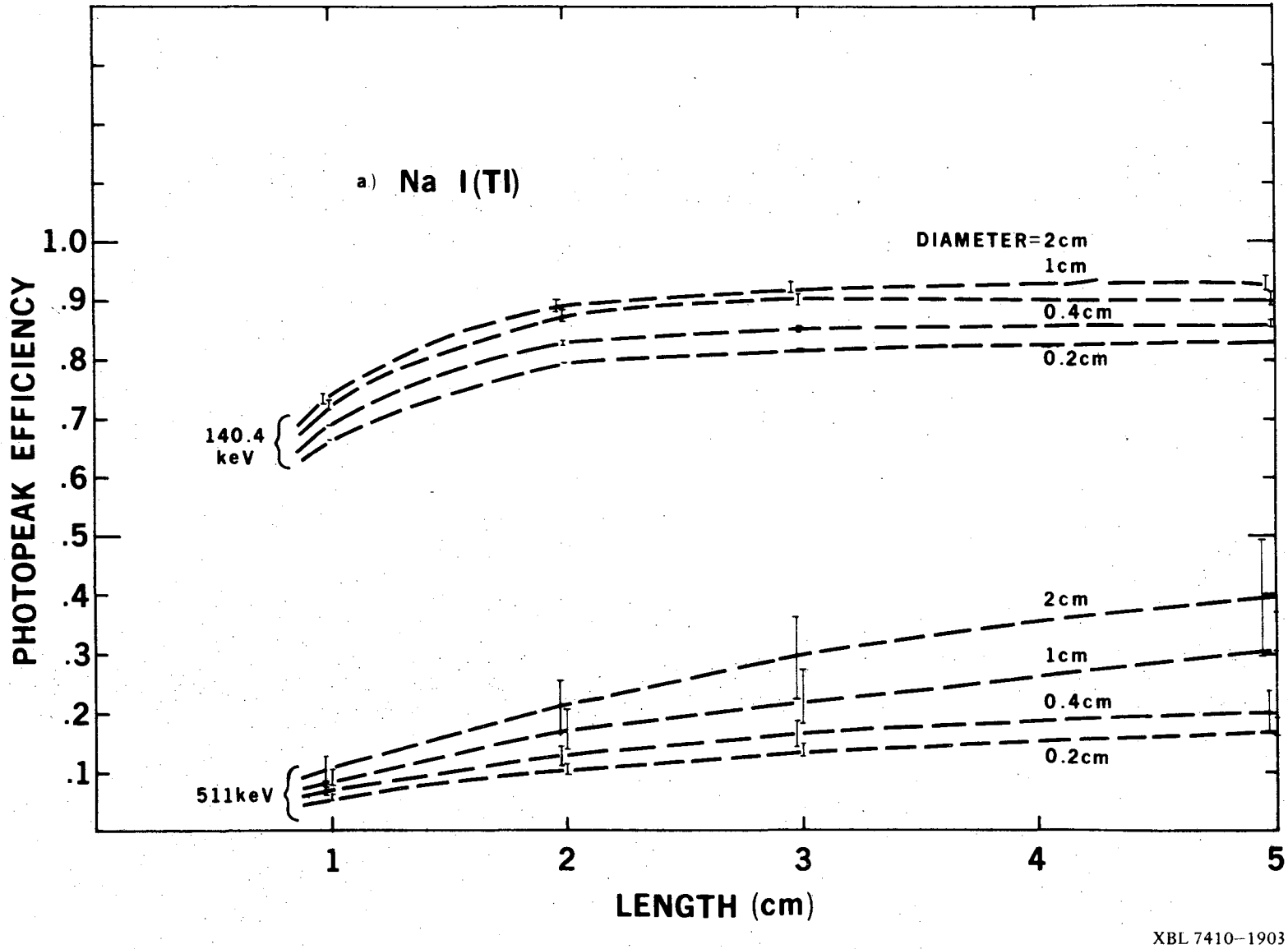

Fig. 23a

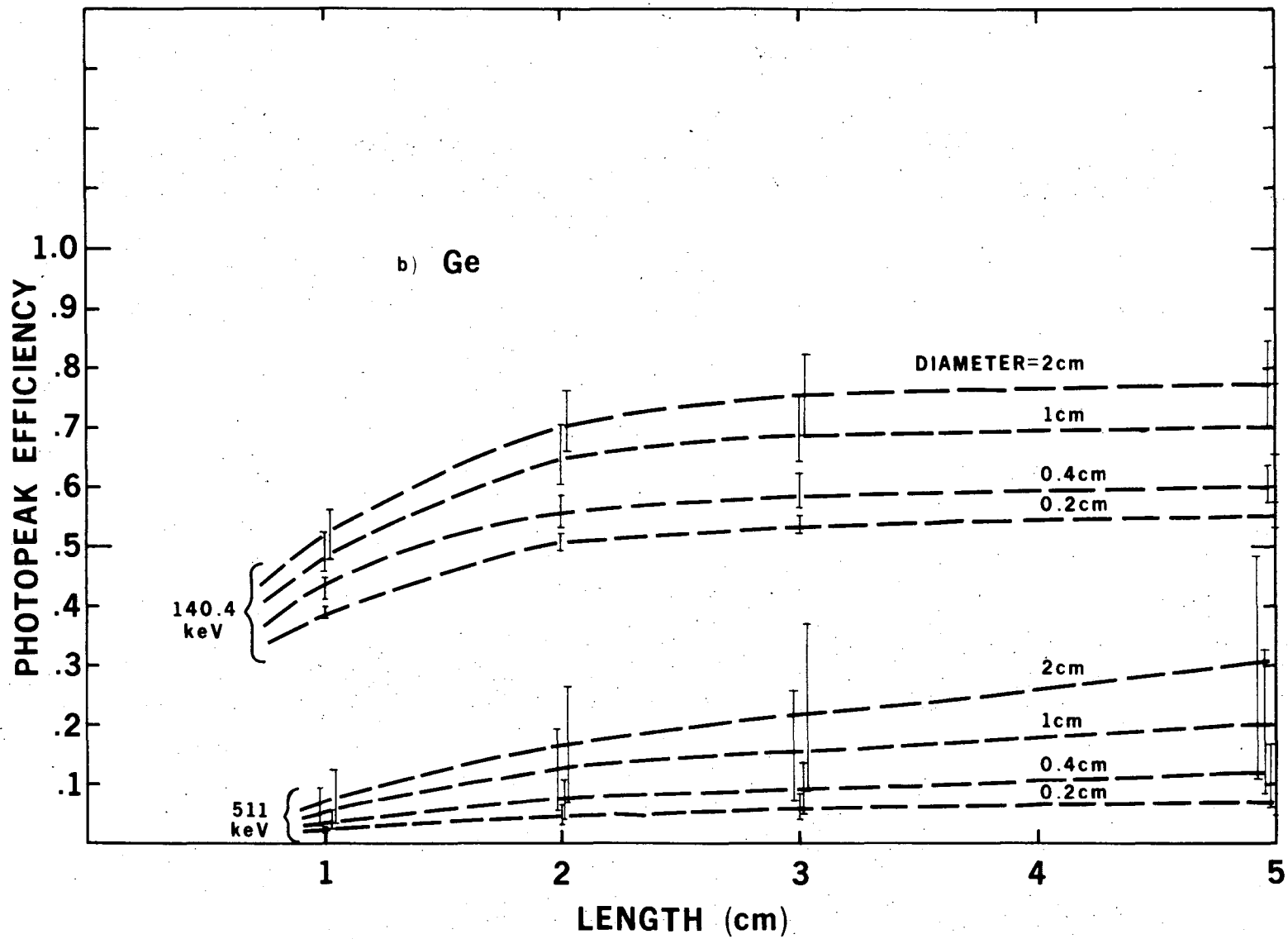
b) Ge
PHOTOPEAK EFFICIENCY
1.0
.9
.8
.7
.6
.5
.4
.3
.2
.1
DIAMETER=2cm
1cm
0.4cm
0.2cm
140.4 keV
2cm
1cm
0.4cm
0.2cm
511 keV
1
2
3
4
5
LENGTH (cm)
XBL 7410-1897

Fig. 23b

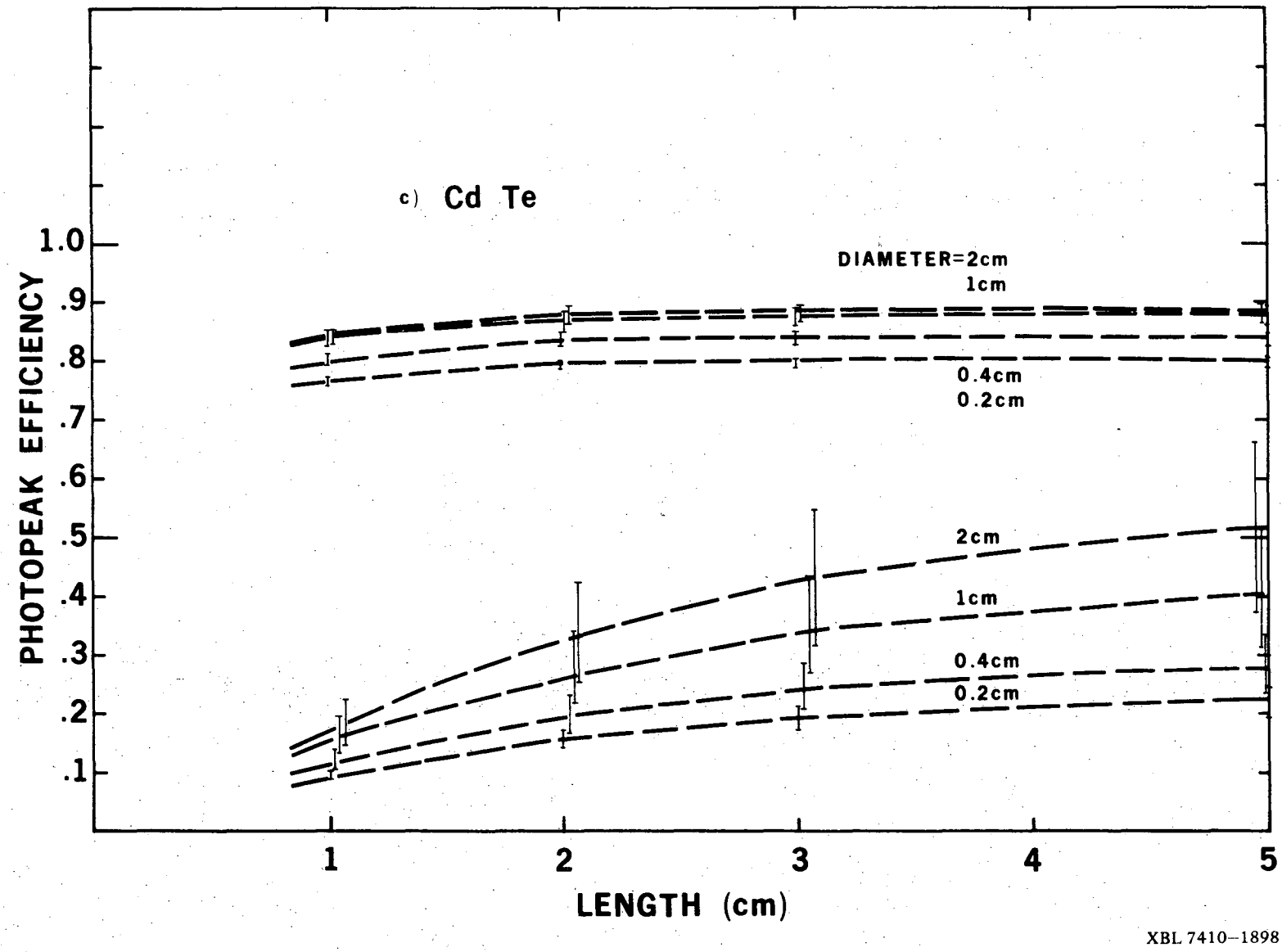

Fig. 23c

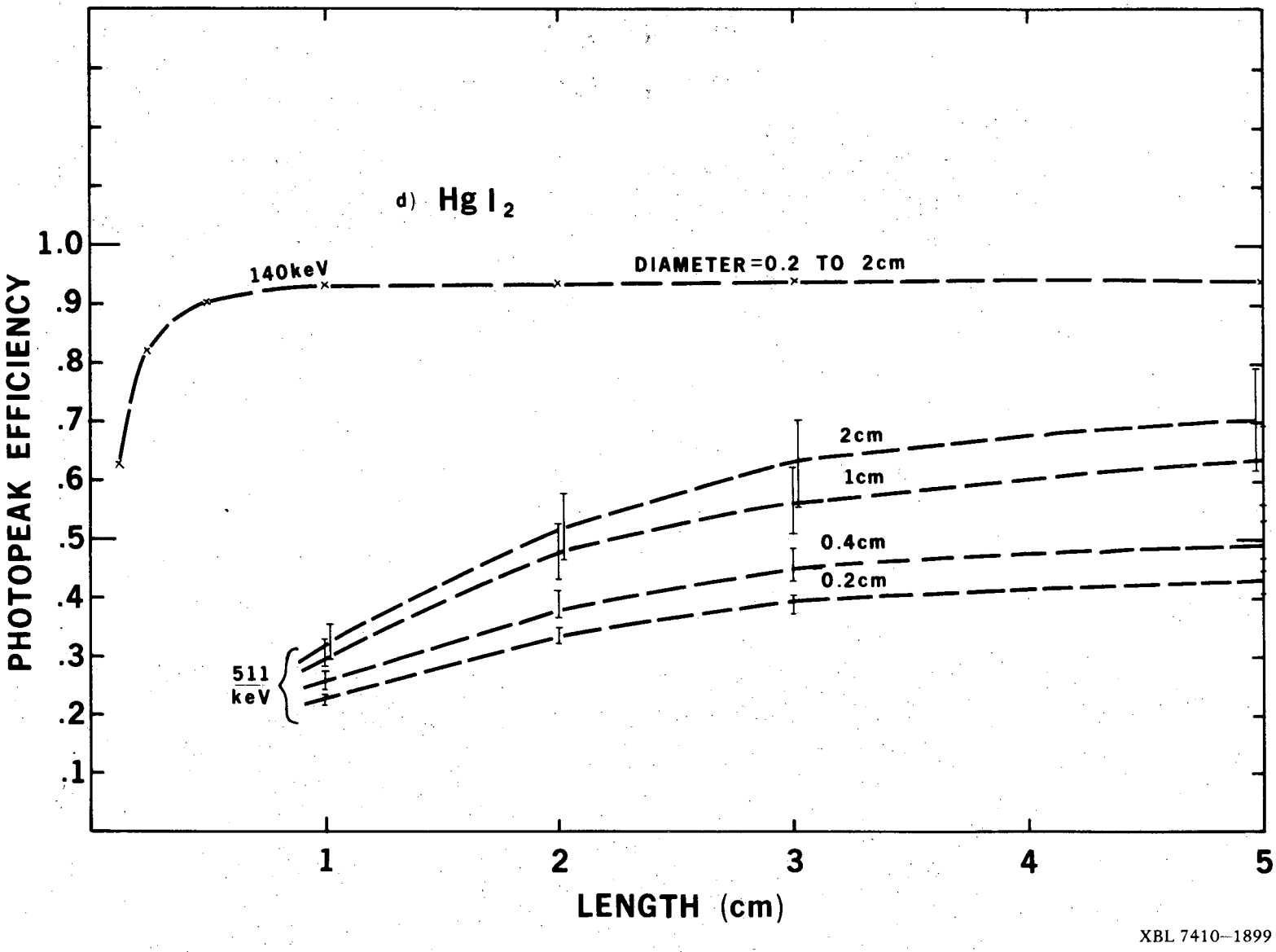
d) Hg I2
PHOTOPEAK EFFICIENCY
1.0
.9
.8
.7
.6
.5
.4
.3
.2
.1
140keV
DIAMETER=0.2 TO 2cm
2cm
1cm
0.4cm
0.2cm
511 keV
1
2
3
4
5
LENGTH (cm)
XBL 7410-1899

Fig. 23d

TECHNICAL INFORMATION DIVISION
LAWRENCE BERKELEY LABORATORY
UNIVERSITY OF CALIFORNIA
BERKELEY, CALIFORNIA 94720